nature neuroscience

REVIEW ARTICLE

https://doi.org/10.1038/s41593-020-00739-8

Recent advances in neurotechnologies with broad potential for neuroscience research

Abraham Vázquez-Guardado[1,8], Yiyuan Yang[2,8], Amay J. Bandodkar[1,3,8] and John A. Rogers[1,2,3,4,5,6,7] ✉

Interest in deciphering the fundamental mechanisms and processes of the human mind represents a central driving force in modern neuroscience research. Activities in support of this goal rely on advanced methodologies and engineering systems that are capable of interrogating and stimulating neural pathways, from single cells in small networks to interconnections that span the entire brain. Recent research establishes the foundations for a broad range of creative neurotechnologies that enable unique modes of operation in this context. This review focuses on those systems with proven utility in animal model studies and with levels of technical maturity that suggest a potential for broad deployment to the neuroscience community in the relatively near future. We include a brief summary of existing and emerging neuroscience techniques, as background for a primary focus on device technologies that address associated opportunities in electrical, optical and microfluidic neural interfaces, some with multimodal capabilities. Examples of the use of these technologies in recent neuroscience studies illustrate their practical value. The vibrancy of the engineering science associated with these platforms, the interdisciplinary nature of this field of research and its relevance to grand challenges in the treatment of neurological disorders motivate continued growth of this area of study.

Neuroscience represents a compelling area for modern research whose goal is to establish an understanding of the principles that underpin complex behaviors in animal species, including ourselves[1]. Successful outcomes will not only contribute to our knowledge of the natural world, but will also have profound consequences in the development of treatment methodologies for neurological diseases[2]. A significant effort focuses on the development of advanced, implantable neurotechnologies as bidirectional interfaces to various parts of the nervous system. When combined with emerging methods in genetic neurobiology, these platforms create a rich range of experimental options in neuroscience research (Fig. 1 and Box 1), particularly for studies that involve freely behaving small animal models as individuals or as interacting social groups. The most mature platforms exist as commercially available wireless systems for electrophysiology and electrical stimulation (e.g., Neuropixels), fiber-optic fluorescence microscopes for imaging neural activity (e.g., Inscopix) and fully implantable, miniaturized light-emitting diodes for neuromodulation (e.g., Neurolux). A parallel set of exploratory efforts revolves around unusual and potentially powerful concepts in neuron-like electrodes[3,4], hybrid biotic–abiotic electrodes[5,6], planar complementary metal-oxide semiconductor systems as platforms for high density electrophysiological mapping[7], injectable bioconjugate nanomaterials as transducing agents for magnetic and/or electromagnetic forms of neuromodulation[8,9] and imaging[10,11], implantable optoelectronic microchips as sources of neuromodulation[12] and minimally invasive components that use ultrasound as wireless power-transfer and communication vehicles for monitoring neural activity[13]. Many of these ideas will likely form the basis of important and widely deployed technologies in the future, perhaps also as enhancements to technologies that represent the core content of this review.

This Review focuses on neurotechnologies that are not yet widely commercially available but that have some strong near-term potential for broad deployment to the neuroscience community based on a set of considerations in device architecture, function and usability; alignment with manufacturing practices; and scope of published examples in animal model studies, both within the originating laboratory and otherwise. The first sections emphasize frontier electrical, optical and pharmacological technologies, with a final passage on the latest developments in synthetic biology and chemistry that may significantly expand the utility of these systems (Box 1). The Review concludes with perspectives on immediate and near-future prospects for continued research activities at the boundaries between neurobiology–chemistry and neuroengineering–technology, along with their implications for the future of neuroscience research.

Platforms for electrical stimulation and recording

Traditional electrical interfaces rely on penetrating probes or flexible sheets with dimensions and electrode configurations that allow recording and/or stimulation across a limited range of spatiotemporal scales. Most technologies adopt relatively simple layouts, nonideal geometries and mechanical properties, with passive designs that cannot easily provide high-resolution mapping capabilities or complementary interfacing methods[14–16]. Recent progress in neuroengineering research and corresponding in vivo validation studies suggest that important alternatives are increasingly available, in various forms and configurations.

Chronically stable integration of integrated electronic systems with soft neural tissues requires high levels of biophysical and

[1]Center for Bio-Integrated Electronics, Northwestern University, Evanston, IL, USA. [2]Department of Mechanical Engineering, Northwestern University, Evanston, IL, USA. [3]Department of Materials Science and Engineering, Northwestern University, Evanston, IL, USA. [4]Department of Biomedical Engineering, Northwestern University, Evanston, IL, USA. [5]Department of Electrical Engineering and Computer Science, Northwestern University, Evanston, IL, USA. [6]Querrey Simpson Institute for Bioelectronics, Northwestern University, Chicago, IL, USA. [7]Department of Neurological Surgery, Feinberg School of Medicine, Northwestern University, Chicago, IL, USA. [8]These authors contributed equally: Abraham Vázquez-Guardado, Yiyuan Yang, Amay J. Bandodkar. ✉e-mail: jrogers@northwestern.edu

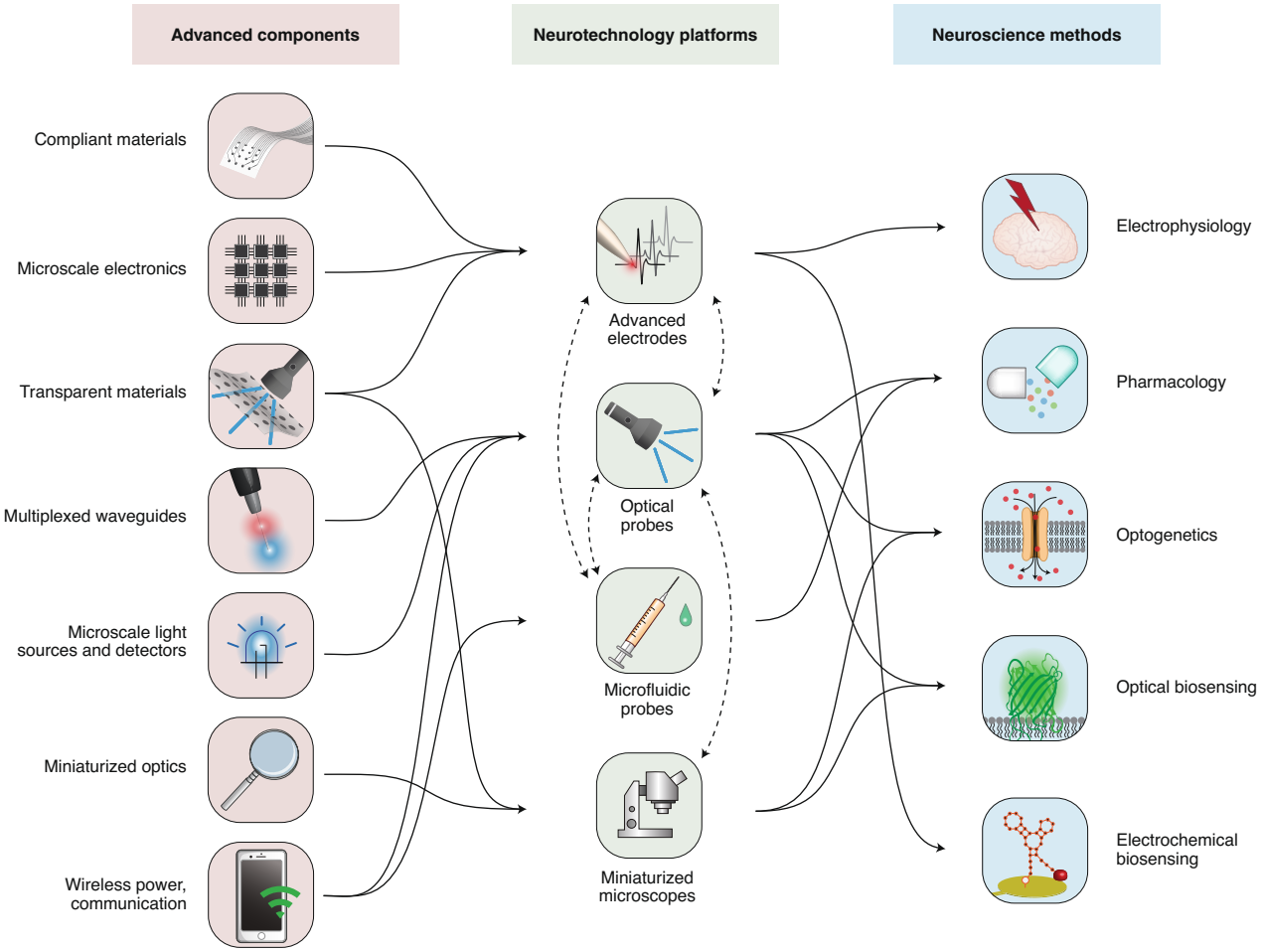

Fig. 1 | Advanced neuroengineering and neurotechnology platforms that support diverse methods in neuroscience. Network scheme that highlights relationships between various neuroscience methods and associated neurotechnology platforms. Advanced engineering components (flexible, stretchable and transparent materials; multiplexed optical waveguides; microscale inorganic light emitting sources and detectors; miniaturized optics; and wireless, battery-free technology) serve as the foundational technologies for biocompatible platforms (advanced electrodes, optical probes, microfluidic probes and miniaturized microscopes: multimodal systems represented as dashed lines) to support existing and emerging methods in neuroscience (electrophysiology, pharmacology, optogenetics, and optical and electrochemical biosensing). The goals are in sophisticated, bidirectional neural interfaces that can be deployed as miniaturized implants in freely behaving animal models, of different sizes, for neuroscience research.

biochemical compatibility to enable uninterrupted operation while in contact with target tissues over timeframes relevant to neuroscience research (days–years)[15]. The large mismatch between the moduli of most conventional electronic materials (tungsten, ~200 GPa; silicon, ~150 GPa) and neural tissues (~1–10 kPa) can lead to physical damage during integration and subsequent use. The resultant chronic inflammatory responses and glial scarring processes degrade the quality of the electrical interface and disrupt the natural state of the biology[17]. A dominating theme for recent neuroengineering research on electrical interfaces is in the development of mechanically compliant platforms, in the form of thin, soft substrates with low bending stiffnesses and ultraminiaturized dimensions[15]. A goal is the development of dense collections of independently addressable electrodes that approach the physical properties, size scales and geometries of neural tissues and cellular networks themselves, with electrical characteristics to enable single-cell resolution[14].

Advances in materials science are essential attempts to achieve sufficiently low interface impedances (characterized at 1 kHz) and physiologically relevant charge-injection capacities (CICs; maximum injectable charge per unit area) for effective, cellular-scale operation in such arrayed formats[18,19]. Techniques that increase the electrochemical surface areas by nanostructuring[20,21] or mixed conduction mechanisms (ionic–electronic) in polymers and nanocomposites are important[22,23]. Examples range from hydrogels doped with poly(3,4-ethylenedioxythiophene):poly(styren esulfonate) (PEDOT:PSS; 0.02 × 1 mm^2 electrode size, 200 nm thickness, 2 Ωcm^2 impedance, 160 mC/cm^2 CICs; Fig. 2a)[22] and gold-coated nanowires of titanium dioxide (Au-TiO_2; 50 × 50 μm^2 electrode size, 3 μm thickness, 0.25 Ωcm^2 impedance, 2.7 mC/cm^2 CICs; Fig. 2b)[20] to platinum–silicone composites (300 μm electrode diameter, 35 nm thickness, 0.5 Ωcm^2 impedance, 57 μC/cm^2 CICs; Fig. 2c)[21] and films of conductive polymer polypyrrole/polycaprolactone-block-polytetrahydrofuran-block-polycaprolactone (PPy/PCTC; 0.5 mm electrode diameter, 15 μm thickness, 60 Ωcm^2 impedance, 48.8 mC/cm^2 CICs; Fig. 2d)[24]. These materials offer significantly lower electrical impedances and higher CICs compared to standard metal counterparts such as platinum (4 Ωcm^2 impedance, 0.5 mC/cm^2)[25] or gold (6.8 Ωcm^2 impedance, 0.4 mC/cm^2 CIC)[25]. In addition, combining these electrical materials with hydrogel supports (modulus ~32 kPa)[22] or thin elastomeric membranes (modulus ~0.4–1.2 MPa)[20,21,24] in strategic layouts guided by mechanics modeling can result in soft, compliant platforms

Box 1 | Technologies and techniques in neuroscience research

Electrodes that form intimate or proximal contacts with neural tissues represent the historical standard as bidirectional interfaces between electronics and the central and peripheral nervous systems[136,137] for purposes of electrical recording and stimulation[138,139]. Progress in the science of the constituent materials and in the engineering aspects of electrical interfaces and embedded electronics serve as the foundations for important recent advances that include miniaturized conformal electrodes and high-performance, low-power electronics. These combined trends are the basis for sophisticated classes of filamentary probes, soft cuffs, flexible sheets, open mesh constructs and other platforms as neural electrophysiological interfaces[14–16]. Such technologies can support high spatiotemporal resolution, with acute and chronic capabilities for engaging neural tissues at scales that span from single cells and even sub-cellular structures to large neuron populations at the level of tissues and organs[140]. Detailed considerations in the arrangements of the electrodes and the excitable tissues can be found elsewhere[19]. These same electrical platforms, complemented with nano-electrochemistry techniques, bioconjugate chemistries and synthetic oligonucleotides, offer greatly expanded ranges of chemical specificity through electroanalytical methods for biochemical sensing[132].

As a complement to electrical forms of neuromodulation, pharmacological manipulation strategies provide a range of additional options in controlling neural behaviors based on endogenous receptors, such as G-protein-coupled receptors[141,142]. Unlike electrical interfaces, these mechanisms support cell-specific operation. Approaches for actively programmed and spatially precise drug delivery in support of this neuromodulation scheme include soft microfluidic networks, miniaturized pumping systems and wireless control strategies, often with supporting electronic components that share materials, methods and functional features with the electrical neural interface systems described above.

Such technologies, particularly when combined with optoelectronic capabilities, serve as the basis of enhanced options in spatiotemporal control when implemented with photoactivatable drugs, as a route for precise, programmable neuromodulation. Here, photolysis converts natively inactive drugs into functional forms upon illumination—a strategy widely used in cancer therapy but with immense potential in neuroscience research[143]. A common scheme employs a photocleavable protecting group that blocks the active moiety of neuropeptides with a chromophore, thereby rendering it inactive. Exposure to high-energy photons (typically ultraviolet) releases the chromophore to activate the neurochemical carrier[143]. Other examples involve synthetic photoswitches, such as photochromic ligands, that undergo reversible photo-isomerization between two or more states upon light irradiation at two characteristic wavelengths. This conformational change alters the binding affinity and/or efficacy toward the target receptor for controlled pharmacodynamics[144]. Such classes of drugs motivate the development of multimodal filaments that, along with drug delivery capabilities, support co-localized, programmable illumination at an infusion site. Electronic, optoelectronic and microfluidic technologies developed in these contexts offer additional value when combined with the most recent techniques in genetic engineering and synthetic biochemistry[145,146]. For example, combination of microfluidics with pharmacogenetic approaches that include designer drugs for targeting specific cells modified with synthetic designer receptors exclusively activated by designer drugs (DREADDs)[147] offer unprecedented selectivity and spatial resolution for neuromodulation.

Optogenetics represents another set of methods in this broader category of cell-specific neuromodulation techniques, but where the mechanisms rely only on light, without a drug component. Here, genetic modifications cause cells to express light-sensitive microbial ion channels, or pumps (opsins), on their membranes to gain light sensitivity[46–48]. Upon illumination with the appropriate excitation wavelength, these opsins modulate ion transmembrane fluxes with millisecond response times, thereby causing either depolarization, associated with transmembrane cation influx (Na^+, ChR2, 470 nm), or hyperpolarization, associated with anion influx (Cl^-, halorhodopsin (HR), 590 nm) or proton outflux (H^+, bacteriorhodopsin (BR), 540 nm). The former leads to stimulation while the latter two result in inhibition[47]. Genetically encoded fluorescent (FL) probes[104,105] support a powerful complementary set of tools to optogenetics and other optical methods that support capabilities in sensing ions[148], transmembrane voltages[149,150] and neurotransmitters[115]. Such genetically encoded FL probes transduce local neural changes into variations in fluorescence that can be captured using local probes or by single-photon or two-photon microscopy techniques.

This review uses engineering features and interfacing modalities as an organizational framework. Figure 1 summarizes the relationships between emerging classes of advanced technology components, their use in neurotechnology platforms and the corresponding capabilities in neuroscience methods. An application perspective represents an alternative and equally valid approach to reviewing the field. For instance, electrical interfaces achieve unprecedented spatiotemporal resolution, even at the single-cell level, but they inherently lack cell-specificity. By contrast, biological and genetic techniques support cell-specificity driven via optical or pharmacological interactions, with timescales in the order of milliseconds to hours, respectively; however, these techniques have poor spatial resolution, limited mainly by drug diffusion or light propagation. Ultimately, the selection among these neural interfaces strongly depends on the research goals, since each has these and other advantages and disadvantages in cell-selectivity, spatiotemporal resolution and scale, degree of invasiveness, duration for stable operation (chronic vs acute) and applicable animal models[14,19,47,104,144].

as neural interfaces, with demonstrated uses that span from small peripheral nerves to large cortical areas[15,26].

Micro- and nanofabrication techniques used in the semiconductor industry can be adapted for application with these unusual materials to produce high-density arrays of electrodes and supporting electronics. Examples are in dense arrays of individually addressable platinum-gold-polymer electrodes (Pt-Au-PEDOT:PSS) on ultrathin polymer substrates (parylene C; thickness 4 μm; modulus 2.7 GPa) with up to 256 cellular-scale electrodes (10×10 μm^2 size, 30 μm spacing, 111×10^3 electrodes/cm^2 resolution, 0.02 Ωcm^2 impedance) for electrophysiological recordings of action potentials of the neocortex and hippocampus of the rat and mid-superior temporal gyrus in humans undergoing epilepsy treatment surgeries (NeuroGrid, Fig. 2e)[27]. The addition of active electronic functionality across such arrays creates opportunities for extreme scaling in density and channel count. High-performance flexible electronics for such purposes use ultrathin (10–500 nm) sheets of silicon as a high quality, flexible semiconductor material for transistors, diodes and other active non-linear electronic components, capable of local amplification, signal aggregation, data processing and multiplexed

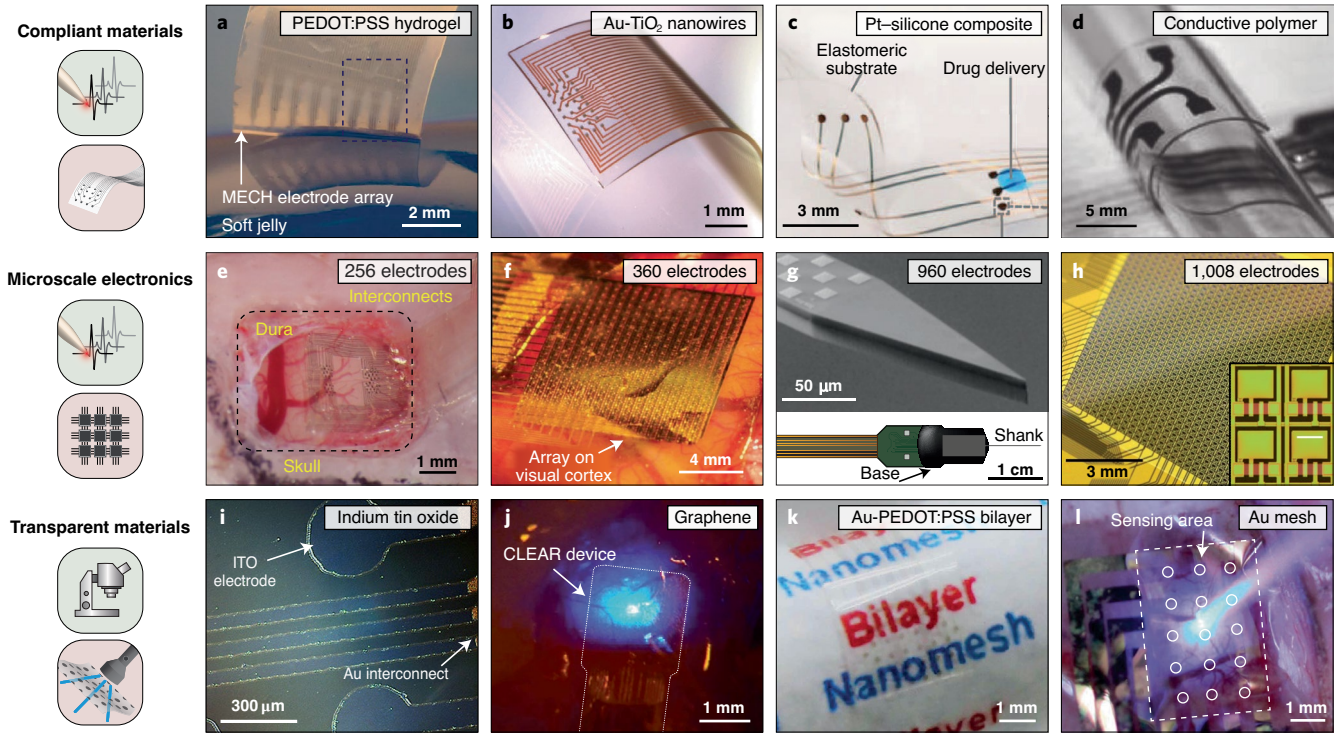

Fig. 2 | Neural interfaces and materials for electrical recording and stimulation. a–d, Mechanically compliant arrays of passive electrodes on thin, flexible sheets. (**a**) Micropatterned hydrogel (MECH) electrodes doped with PEDOT:PSS and integrated on a fluorinated elastomer for stimulation of peripheral nerves. (**b**) High-density, gold-coated titanium dioxide ($Au\text{-}TiO_2$) nanowires as electrodes on a silicone substrate for recording from the cortex. (**c**) Platinum (Pt) nano- and microparticle silicone composite electrodes integrated on a silicone substrate for stimulation of the spinal cord. (**d**) Conductive polymer polypyrrole/polycaprolactone-block-polytetrahydrofuran-block-polycaprolactone (PPy/PCTC) electrodes formed on an elastomeric substrate for recording from the gastrocnemius and for stimulating contractions of skeletal muscles. **e–h**, High density arrays of electrodes in active and passive systems on flexible sheets and penetrating probes. (**e**) Thin (4 µm), flexible array of 256 Pt-Au-PEDOT:PSS electrodes (10 × 10 μm^2, spaced by 30 µm) for recording from cortical neurons at a density of 111 × 10^3 electrodes cm^{-2}. (**f**) Flexible array of 360 gold electrodes (300 × 300 μm^2, spaced by 500 µm) supported by a backplane of active matrix electronics on a thin (25 µm) polyimide substrate for micro-electrocorticography (10 × 9 mm^2) from the auditory cortex at a density of 20 electrodes cm^{-2}. (**g**) Penetrating probe (shank: 10 mm (l) × 70 µm (w) × 20 µm (h)) that supports 960 electrodes (12 × 12 μm^2, spaced 25 µm apart) with integrated complementary metal-oxide semiconductor electronics for low-noise amplification, multiplexing and digitalization of signals from multiple layers of the brain at a density of 160 × 10^3 electrodes/cm^2. (**h**) Kiloscale (1,008 electrodes) capacitive-coupled array of electrodes (195 × 270 μm^2, spaced 250 µm and 330 µm apart vertically and horizontally, respectively) supported by a backplane of active matrix electronics on a thin (47.5 µm) polyimide–elastomer substrate for micro-electrocorticography (9 × 9.24 mm^2) from the cortex at a density of 1,212 electrodes cm^{-2}. **i–l**, Optically transparent arrays of electrodes. (**i**) Arrays of electrodes of indium tin oxide (ITO) on a thin (5 µm) parylene substrate, with transmission of ~75% at a wavelength of 550 nm for optogenetics and electrical recording from the primary visual cortex. (**j**) Carbon-layered electrode array (CLEAR) of graphene on a thin (15 µm) parylene substrate, with transmission > 90% across a range of wavelengths from 400 to 1,400 nm for optogenetics and recording from the somatosensory cortex. (**k**) Arrays of Au-PEDOT:PSS electrodes patterned into mesh structures on a thin (10 µm) parylene substrate, with transmission of ~70% at a wavelength of 550 nm for two-photon imaging and electrical recording from the visual cortex. (**l**) Transparent organic electrochemical transistors interconnected with mesh structures of gold on a thin (1.2 µm) parylene substrate, with transmission of 60% at a wavelength of 550 nm for optogenetics and electrical recording from the cortex. Panels reproduced with permission from: **a**, ref. [22], Springer Nature; **b**, ref. [20], Wiley; **c**, ref. [21], AAAS; **d**, ref. [24], Wiley; **e**, ref. [27], Springer Nature; **f**, ref. [30], Springer Nature; **g**, ref. [29], AAAS; **h**, ref. [34], Springer Nature; **i**, ref. [36], IEEE; **j**, ref. [37], Springer Nature; **k**, ref. [39], AAAS; **l**, ref. [40], PNAS.

readout in scalable architectures[28–30]. An early example comprises an array of 360 recording sites (300 × 300 μm^2 size, 500 µm spacing, 18 Ωcm^2 impedance at 1 kHz) on a thin polyimide substrate (12.5 µm, modulus 4 GPa), for fast addressing with only 38 interconnection lines and sampling rates of ~277 kHz per channel in micro-electrocorticography (Fig. 2f)[30]. The most recent embodiments incorporate 1,008 capacitively coupled electrodes (195 × 270 μm^2 size, 60 µm spacing, 42 $k\Omega cm^2$ impedance) on similar flexible substrates, with sampling rates of 781.25 Hz per channel, distributed over areas approaching ~1 cm^2 (Neural Matrix, Fig. 2h)[28,29]. Here, ultrathin (~900 nm) layers of dense, thermally grown silicon dioxide define capacitive interfaces and also serve as robust biofluid barriers for stable chronic (years) operation, with demonstrations in both rats and non-human primates (NHP). Other platforms leverage wafer-based complementary metal-oxide semiconductor integrated circuit technologies similar to those found in consumer electronics[31–34], for penetrating silicon probes (modulus 150 GPa) with titanium nitride electrodes arranged in 960 channels (12 × 12 μm^2 size, 15 µm spacing, 0.2 Ωcm^2 impedance) at sampling rates of up to 30 kHz per channel along ~1 cm long shafts with 70 × 20 μm^2 cross section (Neuropixels, Fig. 2g)[34,35].

Another area of progress is in the development of transparent conductors to allow simultaneous use of optogenetics, fluorescence wide-field microscopy and two-photon microscopy (TPM). Examples include indium tin oxide (200 µm diameter, 0.1 µm thickness; Fig. 2i)[36], single- or few-layer sheets of graphene (110 µm

diameter; 0.3 nm layer thickness; Fig. 2j)[37], where optical transmittances are 70% and 90%, sheet resistances are 12 Ω/sq and 76 Ω/sq, and interface impedances are 1.6 Ωcm^2 and 19 Ωcm^2, respectively. Arrays of transparent penetrating electrodes (1.5 mm long, 0.4 mm spacing, 125 μm base diameters) formed in transparent zinc oxide (0.15 Ωcm resistivity; refractive index ~2) and coated with parylene C (refractive index ~1.6) as a cladding layer support optical wave-guiding for localized illumination and simultaneous electrical recording (~200 kΩ impedance) at depths of up to 1.5 mm into the brain[38]. Alternative approaches employ fine mesh structures of thin conductive films, where the pattern geometry (for example, filling fraction and thickness) determines its optical and electrical characteristics[39]. With this strategy, hexagonal holey (Au-PEDOT:PSS, electrode diameter 20 μm, 22% filling fraction, unit cell period 1 μm, thickness 25–85 nm, sheet resistance 3 Ω/sq; Fig. 2k)[39] and square mesh (Au; electrode size 70 × 20 μm^2, 30% filling fraction, unit cell period 18 μm, thickness 70 nm, sheet resistance not reported; Fig. 2l)[40] structures defined by colloidal sphere lithography and traditional photolithography achieve transparencies of 70% and 60% and interface impedances of 1.63 Ωμm^2 and 0.14 Ωμm^2, respectively.

These advances in materials, electronics and system designs enable important classes of neuroscience studies. For example, recordings of neuronal activity using a 64-channel NeuroGrid placed on the somatosensory cortex in rats provide insights into non-rapid eye movement (NREM) sleep behaviors[27]. Experimental data show that the rate of firing of cortical neurons decrease at the valley of low-frequency theta oscillations and that these rates are phase-locked to sleep spindle waves (Fig. 3a). Such synchronized, synaptically coupled neuronal activities characterize certain sleep states, such as NREM[41]. In addition, micro-electrocorticography data obtained from human patients during epilepsy surgery yield information on local neuronal activity dysfunction associated with clinical conditions of epilepsy[27].

High-density, large-area systems such as the Neural Matrix extend such capabilities in monitoring of local neuronal activity as well as collective behaviors of neural populations across the brain. Representative results include evidence of synchronization via brain waves[42], spanning neural processes that involve both the sensory and motor cortices for motor task planning[43]. Initial experiments reveal neural activity in NHP models at unmatched levels of resolution and areal span, to confirm the long-range interplay involved in visual stimulation leading to planning and execution (Fig. 3b)[29]. Such studies can be conducted in acute or chronic investigations, where results in rat models demonstrate stable operation over periods of years.

The Neuropixels probe provides complementary features in mapping neuronal activity across multiple functional layers, for studies of perceptual decisions based on sensory stimulus, task planning and execution in freely behaving animals[34,44]. Impressive results of mapping of nearly 30,000 neurons collected from 92 probes in 10 mice across 42 different brain regions using 2 or 3 electrodes per session (Fig. 3c) show that (i) neuronal activity occurs in restricted visual pathways, including the classical visual areas, (ii) neurons that encode non-selective actions are distributed globally and (iii) neurons involved in choice selection are rare and widely distributed, with unilateral encoding in the midbrain and bilateral in the forebrain. Although these results are impressive, extending such measurements to multiple sites with freely behaving animals in experiments that last for months represents a considerable technical challenge.

Transparent electrical interfaces support additional options. In one case, a microelectrode array containing 32 recording sites formed with a perforated bilayer of Au-PEDOT:PSS (Fig. 2k)[39] allows for study of sensory-evoked activity in the visual cortex that leads to increased arousal levels in mice, distinct from quiescence and locomotion states[45]. Recent experiments show that these types of transparent microelectrode arrays can capture electrophysiological signals over a broad frequency band across the primary visual cortex during single-neuron TPM Ca^{2+} imaging with GCaMP during visual stimulation (Fig. 3d). The results suggest that enhanced neuronal activity in the alpha to ultrahigh gamma bands correlates with an increase of single-neuron Ca^{2+} signals and corresponding pupil dilatation behaviors, as neurological evidence of increased arousal[45].

Platforms for optical stimulation and recording

Advances in neuroengineering also address experimental needs in active optical interfaces. Optogenetics is a prominent example that employs transgenic modification[46] of specific types of neurons to express light-sensitive ion channels, or opsins[47,48]. These manipulations allow for optical excitation or inhibition of neuronal activity using advanced probes that deliver light to localized regions with minimum tissue trauma during insertion and chronic use[48]. Locally averaged measurements or full spatial imaging of neuronal activity enabled by FL indicators represent additional forms of optical interfaces that can be supported by similar technologies, to complement the control mechanisms provided by optogenetics.

Standard fiber optic cables and fixtures adapted from the telecommunication industry represent the simplest mechanism for performing optogenetics and localized fluorescence measurements (commonly referred to as photometry)[49]. Disadvantages in animal studies include requirements for physical tethers to external light sources and/or detectors, nonideal coupling of high-modulus glass waveguides (~50–90 GPa) to soft neural tissues (~1–10 kPa) and limited options for light collection and delivery. Structured and tapered fibers (TF) overcome this last drawback by engaging large, selected neuron populations with certain levels of spatial control via multi-wavelength volumetric[50,51] or multisite illumination and collection[52]. In certain TF cases, multimode fibers allow mode-division demultiplexing (MDD) from small taper angles at the tip (~3–6°) that also minimize tissue damage[50–52]. Different waveguide modes, selectively excited at the back end of the fiber, escape at different sections of the taper, to support selective multi-wavelength illumination at different depths of the brain[51,52]. Figure 4a shows a representative multipoint emitting optical fiber that delivers optical stimulation to seven different emission windows (~20 μm) using MDD[52]. These windows can also selectively collect fluorescence signals, to allow both spatially resolved optogenetic stimulation and photometry in a single fiber[50]. An alternative relies on planar waveguides, lithographically defined on flat silicon shanks (thicknesses <50 μm), and wavelength-division demultiplexing (WDD) techniques, to direct light to multiple cellular-scale out-coupling illumination zones (Fig. 4b)[53,54].

Other types of probes eliminate the need for a tethered optical waveguide by using microscale inorganic light emitting diodes (μ-ILEDs) as tissue-embedded illumination sources that can also support components for sensing and/or other forms of neuromodulation[55,56]. In one example, silicon probes (70 μm wide, 30 μm thick, 5 mm long) include small arrays of indium-gallium nitride μ-ILEDs (10 × 15 μm^2) to deliver illumination at single-neuron resolution to targeted locations in the brain, with intensities of up to ~350 mW/mm^2. An associated set of titanium-iridium electrodes (11 × 13 μm^2, impedance 1.43 Ωcm^2) on the same platform offer capabilities in simultaneous electrophysiological recording (Fig. 4c)[57], with tethers only for power and data acquisition.

As with electrical interfaces, compliant materials offer additional advantages, particularly for chronic operation with minimal tissue disruption[58]. Flexible probes that combine cellular-scale electronic and optoelectronic components on thin, narrow polymer fibers are of particular interest[59]. Figure 4d shows an example in which a polyester filament (20 μm thick) serves as a substrate for four μ-ILEDs

(50 × 50 μm², 6.45 μm thick), each of which produces an intensity of up to 40 mW/mm² (ref. [60]). The addition of microscale inorganic photodetectors (μ-IPDs; 200 × 200 μm², 1.25 μm thick), thin-film Pt electrodes and temperature sensors in a multilayer configuration enables multimodal operation with minimal increases in the size of the probe (Fig. 4e), for comprehensive monitoring of neural activity and responses to optical stimulation.

A key additional feature of these technologies follows from the integration of miniaturized components that support radio frequency resonant wireless power-transfer and control for studies of freely moving animals in naturalistic conditions and in social groups, without constraints from any type of tether, whether optical, electrical or otherwise[61–69]. In fact, the most advanced systems (Fig. 4f) can be used as complete subdermal implants[61], in the form of thin (~500 μm), flexible units that can operate for years without degradation or any measurable impact on animals' locomotor or neurological behaviors[66,67]. A typical device contains a receiving antenna, a probe with at least one commercial μ-ILED (270 × 220 μm², 50 μm thick) near the tip end for optogenetic stimulation, a collection of low-power, small-form electronic components mounted on flexible printed circuit boards and an encapsulating structure formed with a bilayer of parylene (14 μm) and polydimethylsiloxane (PDMS; ~30 μm)[61]. The latest designs allow independent user-definable control over intensity, frequency and duty cycle at different wavelengths, with multiple μ-ILEDs[70]. These platforms apply to broad classes of animal models, not only in the brain but also at other locations of the central and peripheral nervous system (Fig. 4g), with minor modifications[64,66,68].

Further elaborations include wireless bidirectional communication capabilities for user control and data streaming from sensors co-located on the same probes[67,71]. The example in Fig. 4h includes a μ-ILED and a μ-IPD to stimulate and record fluorescence signals, respectively, associated with calcium indicators in the vicinity of the probe[71]. A microcontroller (3 × 3 mm²) synchronizes stimulation and recording and initiates wireless data transmission using an infrared optical communication link at sampling rats of 27 Hz and 12-bit precision. This miniaturized system can be deployed as a tether-free subdermal implant not only for calcium recording, but also for examining other neurochemical dynamics transduced by genetically encoded FL probes. Additional versions of such devices integrate a pair of μ-ILEDs and a μ-IPD for local measurements of blood oxygenation in neural tissue[72].

Incorporating lenses and imaging systems in compact geometries expands recording capabilities from local interfaces at one or

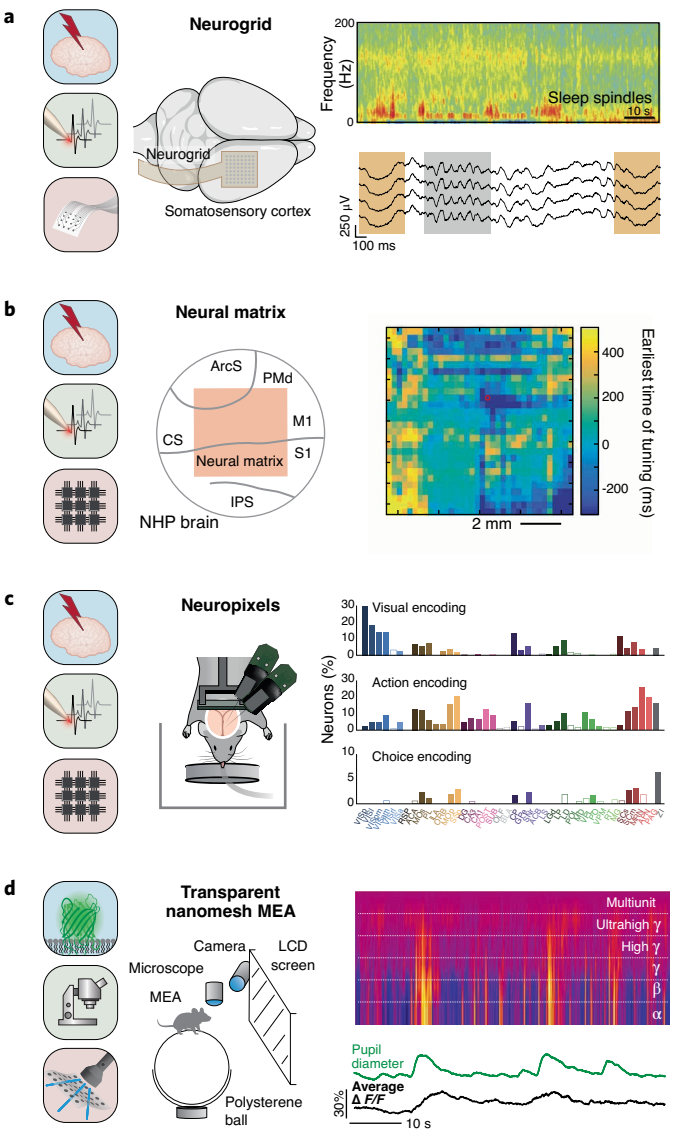

Fig. 3 | Uses of advanced platforms for electrical recording and stimulation in neuroscience research with small and large animal models. a, Application of the Neurogrid technology for recording of local field potentials (LFPs) from 64 electrodes on the somatosensory cortex in anesthetized rats. The results provide insights into neuronal activity associated with non-rapid eye movement (NREM) sleep behavior. Left: schematic illustration of the placement of the Neurogrid. Right: color-coded spectrogram (warmer colors correspond to high powers) of representative LFPs (raw traces in the bottom panel) from the cortex, highlighting sleep spindles in the 9–16 Hz frequency band (gray area) and slow oscillations in the 2–4 Hz frequency band (orange area). **b**, Application of the Neural Matrix for high-resolution recording across large areas of the cortex in NHPs. This kiloscale, multiplexed microelectrode array reveals large-scale neuronal synchronization of sensory and motor cortices during motor task planning. Left: schematic illustration of the placement of the Neural Matrix over an area of ~1 cm² across the targeted primary sensory regions: arcuate sulcus (ArcS), central sulcus (CS), intraparietal sulcus (IPS), dorsal premotor cortex (PMd), primary motor cortex (M1), and primary sensory cortex (S1). Right: spatial map representing the time interval when the directional tuning first becomes statistically significant ($P < 0.05$) for each electrode. These results show the temporal evolution of directional information, which starts in focal areas of the premotor cortex and then shifts first to the primary motor and then to sensory cortices. **c**, Application of the Neuropixels technology for the study of brainwide neuronal activity of perceptual decisions during sensory stimulus, task planning and execution in awake, behaving and head-fixed mice. The data correspond to recordings from nearly 30,000 neurons, captured with 92 probes in 10 mice across 42 brain regions. Left: schematic illustration of the experimental setup, showing two Neuropixels probes inserted in the brain during each recording session. Right: histogram of neuronal spiking across 42 regions of the brain, showing the diversity of neural activity during visual, action and choice encoding. A list of acronyms is found in ref. [44]. **d**, Application of an optically transparent Au-PEDOT:PSS microelectrode array (MEA) for the study of arousal states in awake, head-fixed mice. Two-photon imaging captures record Ca^{2+} dynamics simultaneous with recording of electrophysiology from the primary visual cortex during visual stimulation. Left: schematic representation of the experimental setup. LCD, liquid crystal display. Right: Spectrogram of recordings from a representative electrode showing the distinct frequency bands involved in neuronal activity during visual stimulation (multiunit, ultrahigh gamma (γ), high γ, γ, beta (β), and alpha (α)). Top: pupil dilatation diameter (green plot); bottom: average Ca^{2+} fluorescence dynamics (black plot). Panels reproduced with permission from: **a**, ref. [27], Springer Nature; **b**, ref. [29], AAAS; **c**, ref. [44], Springer Nature; **d**, ref. [39], AAAS.

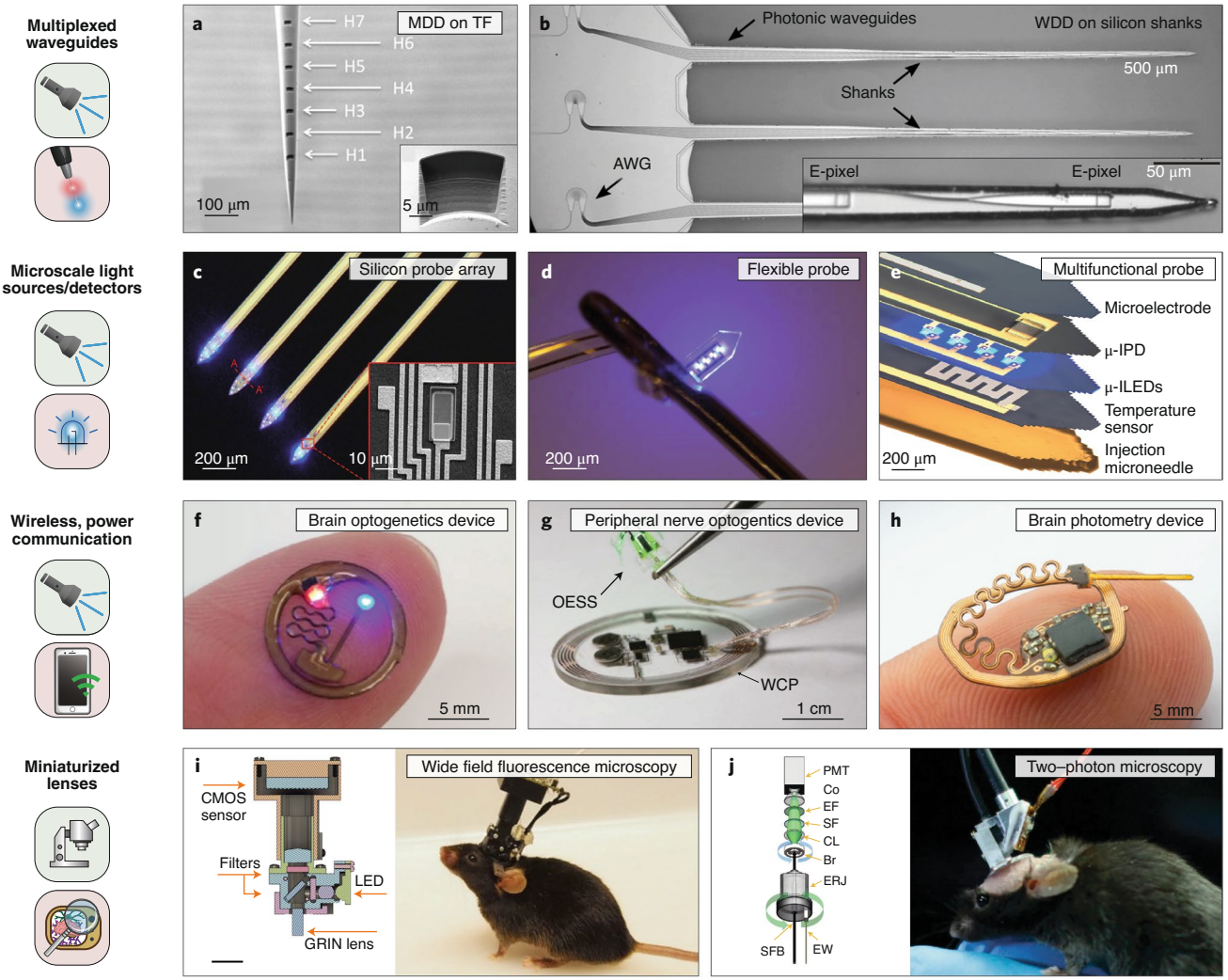

Fig. 4 | Neural interfaces for optical stimulation, recording and imaging. a,**b**, Advanced waveguide structures for optical delivery and sensing. (**a**) Scanning electron microscope (SEM) images of a TF for optogenetic stimulation at seven optical output ports addressable by MDD. Inset: magnified view of an output port (~20 μm). (**b**) Optical image of planar waveguide arrays on silicon probes (shanks), addressable by wavelength-division demultiplexing (WDD) via arrayed waveguide gratings (AWG) to deliver light to multiple regions of the brain. Inset: magnified view of two 10 × 10 μm^2 light output ports (E-pixel) along the waveguide. **c**–**d**, Implantable μ-ILEDs and μ-IPDs. (**c**) Optical microscope and SEM images (inset) of silicon probes (5 mm (l) × 70 μm (w) × 30 μm (h)) that each includes three μ-ILEDs (10 × 15 μm^2) and eight titanium–iridium electrodes (11 × 13 μm^2) for optogenetic stimulation and electrophysiology recording, respectively. (**d**) Photograph of a polyester neural probe (~20 μm thick) with four μ-ILEDs (50 × 50 μm^2, 6.45 μm thick, 40 mW/mm^2 irradiance at the surface) for optogenetic stimulation, threaded through the eye of a sewing needle and wrapped around its shaft to illustrate the mechanical flexibility and the size scale. (**e**) Exploded view illustration of a multifunctional neural probe in a multilayer geometry. The probe includes (from top to bottom) a platinum (Pt) electrode (20 × 20 μm^2) for electrophysiological recordings, an μ-IPD (200 × 200 μm^2, 1.25 μm thick) for optical measurements, four μ-ILEDs (50 × 50 μm^2, 6.45 μm thick) for optogenetic stimulation, a serpentine Pt resistor for temperature sensing and a removable injection microneedle (250 μm). **f**–**h**, Wireless, battery-free, fully implantable platforms (**f**). Subdermal head-mounted optogenetic device with radio frequency power harvesting and control for operation of a μ-ILED (270 × 220 μm^2, 50 μm thick) at the tip of a flexible polyimide probe for optogenetic stimulation. (**g**) Subdermal device for peripheral optogenetic neuromodulation, which consists of an optoelectronic stimulation and sensing (OESS) module and a wireless control and power (WCP) module for closed-loop regulation of bladder function. (**h**) Subdermal head-mounted photometry device with radio frequency power harvesting and control for operation of a μ-ILED (270 × 220 μm^2, 50 μm thick) and data transmission from a μ-IPD (300 × 300 μm^2, 100 μm thick) for optical recording of calcium dynamics. **i**,**j**, Imaging platforms based on external head-mounted microscopes. (**i**) Wide-field microscope for fluorescence imaging. Left: cross-section diagram. Right: in vivo operation. CMOS, complementary metal-oxide semiconductor electronics; GRIN, gradient index. (**j**) Two-photon microscope for fluorescence imaging. Left: schematic illustration of the device designs. PMT, photomultiplier; Co, condenser; EF, emission filter; SF, short-pass filter; CL, collection lens; Br, bearing; ERJ, electrical rotary joint; EW, electrical wires; SFB, supple fiber bundle. Right: in vivo operation. Panels reproduced with permission from: **a**, ref. [52], Elsevier; **b**, ref. [53], SPIE; **c**, ref. [57], Elsevier; **e**, ref. [60], AAAS; **f**, ref. [61], Elsevier; **g**, ref. [64], Springer Nature; **h**, ref. [71], PNAS; **i**, ref. [74], Springer Nature; **j**, ref. [76], Springer Nature.

several brain regions to widefield spatiotemporal visualization of neuronal activity[73]. As extensions of commercial widefield fluorescence microscopes that use head-stages (Fig. 4i)[74,75] for volumetric imaging (~700 × 600 × 360 μm^3) at high sampling rates (16 Hz) and fine resolution (~15 μm)[76], TPM offers significant enhancements in spatial resolution and reduction in background noise with similar form factors (Fig. 4j)[77]. TPM operation exploits a raster scanning process enabled by optical and micro-electromechanical

components to excite fluorophores across volumetric elements (voxels) with near infrared femtosecond pulses (~100 fs, 920 nm) delivered through hollow-core photonic crystal fibers[72,78,79]. Figure 4j shows a head-mounted device of this type, with lateral resolution of 0.64 μm, axial resolution of 3.35 μm and 40 Hz sampling rate for a field of view (~130 × 130 μm^2) that includes 256 × 256 pixels (ref. [76]. Recent work demonstrates that TPM techniques can also realize spatially resolved optogenetic excitation of selected neurons. Combining these two approaches allows simultaneous modulation and recording of neural activity among selected neurons across different brain depths[80,81], although with requirements for tethers to external hardware.

Recent applications of these technologies in neuroscience research demonstrate important, unique capabilities in animal models. The TF, MDD and wavelength-division demultiplexing approaches for optical fibers described previously expand options in illumination volume[82] and dynamic multisite light delivery[51,52]. In one example, a TF provides large-volume optogenetic inactivation of frontal eye field neurons (over 10 mm^3) in a NHP, as a means to investigate relationships between different aspects of frontal eye field activity and memory-guided eye movements[83]. Another study exploits multisite illumination of TF using MDD to achieve dynamic optical stimulation of indirect pathway striatal projection neurons between ventral and dorsal striatum in mice to examine their effects on locomotion (Fig. 5a). Simultaneous ventral and dorsal striatum stimulation results in reduced locomotion and triggered contraversive spinning, while ventral stimulation alone leads to a more profound decrease in traveled distance (Fig. 5a)[51].

As another example, probes that combine μ-ILEDs with microelectrodes allow optogenetic excitation of small numbers of pyramidal cells and simultaneous measurements of action potentials of surrounding interneurons in a hippocampal network to examine monosynaptic pairwise interactions[84]. The cross-correlograms of 118 pyramidal cell–interneuron pairs exhibit similar and highly correlated spike transmission probabilities under optical evocation compared to the spontaneous scenario, suggesting pairwise interactions between these two cell types (Fig. 5b). Meanwhile, a significantly higher spike transmission during optical evocation compared to baseline indicates that more than one pyramidal cell drives the same interneuron.

Fully implantable, wireless, battery-free platforms of this general type offer unique options in freely behaving animals. This technology supports protocols in complex environments, in social groups and in interfaces with parts of the anatomy that are cumbersome with external wiring. One example explores the regulation of nocifensive behaviors through optical excitation of the transient receptor potential vanilloid 1 (TRPV1) afferents at the L4–L6 spinal cord segments in mice[66]. Optical activation produces reversible pain behavior (Fig. 5c), highlighting the roles and mechanisms of these afferents. Combined with wireless communication and data streaming from integrated sensors, these devices can also support real-time photometry of neural activity. A recent demonstration examines

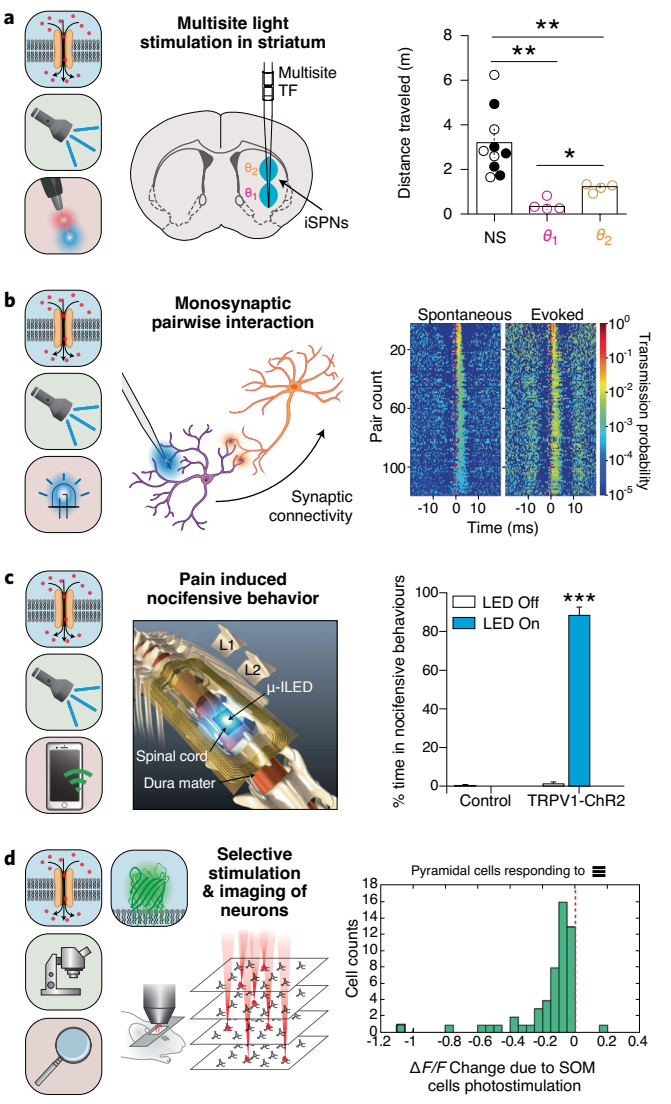

Fig. 5 | Uses of advanced platforms for optical recording and stimulation in neuroscience research with small animal models. a, Application of TF for multisite optogenetic stimulation in the striatum of a mouse model expressing ChR2-YFP in indirect pathway striatal projection neurons (iSPNs). Dynamic optical stimulation between ventral and dorsal striatum by mode-division demultiplexing (light input at θ_1 magenta = 8°, ventral; θ_2 orange = 22.5°, dorsal) allows studies of their effects on locomotion. Left: schematic illustration of the placement of the TF. Right: distance traveled during a 3-min session of no stimulation (NS), ventral stimulation (θ_1) and dorsal stimulation (θ_2). **b**, Application of silicon neural probes with inorganic μ-ILEDs and associated electrodes. Optogenetic excitation of small numbers of pyramidal cells and simultaneous measurements of action potentials of surrounding interneurons in the hippocampal network yields information on monosynaptic pairwise interactions between these two cell types. Left: cartoon rendering of the probe and its interaction with neuronal projections. Right: cross-correlograms (CCG) of 118 paired activations between pyramidal cells and interneurons during spontaneous and optogenetically evoked scenarios. **c**, Application of fully implantable wireless, battery-free platforms for optogenetic stimulation of the spinal cord. Optogenetic excitation of the transient receptor potential vanilloid 1 (TRPV1) afferents at the L4–L6 spinal cord segments in mice regulates nocifensive behaviors. Left: schematic illustration of the device and its interface to the spinal cord. Right: time during nocifensive behaviors of non-transgenic mice (control) and TRPV1-ChR2 mice. **d**, Application of head-mounted devices for TPM. TPM-enabled selective activation of somatostatin (SOM) interneurons concurrently among three brain planes (~50 μm vertical separation, 200 × 200 μm^2 planar dimension) in layer 2/3 of the primary visual cortex (V1) and simultaneous measurement of calcium activity of surrounding pyramidal cells in mice allows studies of their interactions. Left: schematic illustration of the setup and the interaction of light with different layers of the brain. Right: histogram of changes in fluorescence ($\Delta F/F$) show that SOM interneuron excitation significantly suppresses pyramidal cell activity in mice when visualizing grating stimuli. Panels reproduced with permission from: **a**, ref. [51], Springer Nature; **b**, ref. [84], Elsevier; **c**, ref. [66], International Association for the Study of Pain; **d**, ref. [80], Yang et al.

Ca^{2+} transients in the basolateral amygdala (BLA) of mice during unpredicted foot-shock[67]. A significantly increased frequency of Ca^{2+} spikes that follows an electrical shock indicates a strong correlation between neuronal activity in the BLA and negative emotions such as fear and anxiety.

Head-mounted imaging systems further extend recording capabilities to spatially resolved maps of neural activity in rodents[85], NHPs[86] and fish[87]. Illustrative results involve imaging of Ca^{2+} activity across up to 240 primary motor cortex (M1) neurons in a 6×4 mm^2 field of view of the left hemispheres of free-behaving marmosets during lever-pulling, ladder-climbing and pellet-reaching tasks to reveal different subsets of participating neurons. An application of TPM as an optogenetic interface explores the effect of stimulation of somatostatin interneurons on the activity of pyramidal cells during visual stimuli in rats. Selective activation of somatostatin interneurons concurrently among three brain planes (~50 μm vertical separation, 200 × 200 μm^2 planar dimension) in layer 2/3 of the primary visual cortex (V1) in mice results in significant suppression in activity of pyramidal cells when visualizing grating stimuli (Fig. 5d)[80].

Technology platforms for programmed pharmacology

Progress in the field of nano- and microfluidic technologies creates opportunities in the development of programmable drug-delivery platforms in the form of implantable and filamentary probes. Enhanced operation follows from the use of miniaturized electronics and wireless communication technologies similar to those described in previous sections. The most advanced systems support precise temporal control of multiple drugs, infused independently over long periods of time with minimal damage to the tissues and in designs that allow for studies of animals behaving naturally.

In one case, a thin silicon shank (9.15 mm long, 1 mm wide, 40 μm thick) supports five redundant microfluidic channels (each 7.5 μm wide, 9 μm thick) for deep brain pharmacological stimulation (Fig. 6a)[88,89]. When integrated with a head-mounted stage and tubing to external fluid-managing systems, this 'chemprobe' can supply up to three drugs individually or simultaneously to the target brain regions at physiologically safe flow rates (110–660 nl/min). One embodiment also incorporates 16 iridium microelectrodes (each 19 × 19 μm^2; 2.8 Ωcm^2 impedance) in the vicinity of the outlet for electrophysiology recordings. The fabrication processes also allow silicon probes with similar functionalities[90], as well as those that include options for optogenetics stimulation[91].

Complex-fiber-type multifunctional microfluidic probes formed using thermal drawing techniques represent alternative platforms and fabrication schemes. A recent construct combines a pair of microfluidic channels (~20 × 20 μm^2), six electrodes (each ~20 × 20 μm^2, 0.8 kΩ/sq sheet resistance, 2.48 Ωcm^2 impedance) of graphite–conductive polyethylene composite and an optical waveguide made of a polycarbonate core (refractive index of 1.586, ~70 μm diameter) and cyclic olefin copolymer cladding (refractive index of 1.53; Fig. 6b)[92]. This multifunctional fiber (200 μm diameter) inserts into the brain and connects via optical fiber, electrical wiring and fluid tubing to external control hardware. The device, driven by the external drug infusion system, delivers small volumes of drugs with flow rates between 60 and 600 nl/min. The polymeric construct has significantly lower bending stiffness (75–80 N/m) compared to metallic cannulas (>5 MN/m) and a much smaller diameter (460 μm diameter for a 26-gauge metal cannula), thereby minimizing tissue damage during insertion and subsequent use.

Recent advances support fully integrated, self-contained devices that eliminate requirements for physical tethering. A dual-functional platform of this type combines programmed pharmacology with optogenetics (Fig. 6c). Recent reports describe battery-powered and battery-free wireless devices, suitable for a broad range of untethered behavioral studies in small animal models[93–98]. In one design, up to four individually addressable, refillable drug reservoirs house drugs that can be pumped at programmed times using electrolytic (flow rate up to 5 μl/min)[94,97] or thermal (flow rate ~1.5 μl/min)[93,95,96] actuators through microfluidic channels (10 × 10 μm^2 cross section) in thin, flexible silicone probes (500 μm wide, 50 μm thick). The low bending stiffness (13–18 N/m) facilitates stable interfaces to the brain[93–96] or, as cylindrical cuffs, to the surfaces of peripheral nerves[97]. Co-located μ-ILEDs (100 × 100 × 6.54 μm^3) at the tips of the probes allow independent optogenetic stimulation and/or photoactivation, in an all-wireless electronic setup as described in Fig. 4e,f.

These collective capabilities for localized pharmacological stimulation can be leveraged for investigations of synaptic pathways via activation and deactivation of targeted excitatory receptors with high cell-specificity, involving localized neural modulation and its projection to other brain regions that define behavior and cognitive paradigms. One study focuses on the hippocampal CA1 and CA3 regions and their contributions to episodic and semantic memory consolidation, memory encoding and retrieval, critical during navigation engagement[99,100]. Experiments use four separate silicon shanks implanted in transgenic mice expressing channelrhodopsin 2 (ChR2) in CA3 (ref. [91]), one multimodal for drug delivery, optogenetic stimulation and electrophysiology recording in CA3, and three others across CA1 and CA3 for electrophysiology recording (Fig. 7a). The results indicate that optogenetic stimulation of CA3 neurons in anaesthetized mice produces neuronal activity patterns that propagate to the CA1 region. The acute infusion in CA3 of the AMPA receptor antagonist 6-cyano-7-nitroquinoxaline-2, 3-dione (CNQX) and NMDA receptor antagonist (2 R)-amino-5-phosphonovaleric acid (AP5) can block this excitatory pathway, as observed in the decay of neuronal activity in CA1 (Fig. 7a), thereby revealing important signaling interrelationships.

Multicomponent polymeric probes that support drug delivery, optogenetic stimulation and electrophysiological recording (Fig. 6b) can be used to explore behaviors in unanesthetized tethered animals[92]. An example involves modulation of the BLA neuronal projections to the ventral hippocampus (vHPC), in the context of fear and anxiety behaviors[101]. Experiments show that optogenetic stimulation of the BLA in mice transfected with ChR2 invokes anxiety, as observed through a reduction of time spent in the center of an open field environment (Fig. 7b). Infusion of CNQX into the vHPC before stimulation blocks synaptic inputs from the BLA, resulting in a decrease in anxiety assessed in this manner. These results demonstrate that glutamatergic inputs in the vHPC from the BLA are responsible for the engagement in such behaviors and that this excitatory pathway can be exploited as a pharmacological route for inhibition[101].

Such options in recording and multimodal neuromodulation are particularly enabling when implemented in fully wireless, tether-free systems, with unique opportunities in animal models that freely interact in naturalistic enclosures. A recent demonstration uses a lightweight head stage system (as in Fig. 6c)[93,94], for programmed, unilateral pharmacological stimulation of the μ-opioid receptor with its agonist [D-Ala^2,*N*-Me-Phe^4,Gly^5-ol]-enkephalin (DAMGO) in the ventral tegmental area to modulate contralateral rotation locomotion in mice (Fig. 7c)[102]. Advanced systems with similar minimally invasive form factors employ bidirectional wireless communication for real-time, closed-loop pharmacological and optogenetic neuromodulation based on dynamic behavioral outcomes[96]. Guided by an artificial vision system, this device induces robust place preference upon optogenetic stimulation of the lateral hypothalamus (LH), which is known to produce projections to the bed nucleus of the stria terminalis (BNST) in mice transfected with ChR2. The programmed infusion of gabazine, the receptor antagonist of the GABA receptors, into the LH robustly inhibits this behavior (Fig. 7d). This finding confirms the role of the BNST–LH in

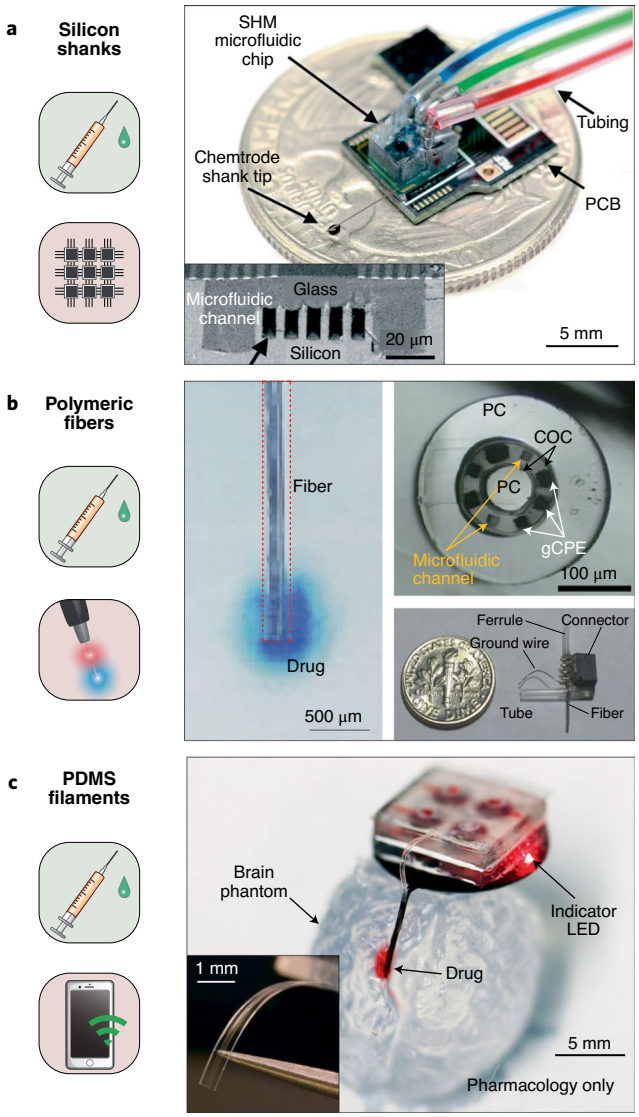

Fig. 6 | Neural interfaces for programmed pharmacology and other advanced functions in neuromodulation. a, Silicon probe (shank; 160 μm wide, 40 μm thick) that supports microfluidic channels (7.5 × 9 μm^2 cross-section) for delivery of three different drugs and 16 iridium electrodes (19 × 19 μm^2) for electrophysiology recordings. PCB, printed circuit board. Inset: scanning electron microscope cross-sectional image of the microfluidic channel structure. **b**, Multifunctional polymeric optical fiber that incorporates capabilities for optogenetic stimulation, pharmacological delivery and electrophysiology recording. Left: delivery of a blue liquid solution in 0.6% agarose gel phantom. Top right: cross-sectional image of the fiber showing the polycarbonate (PC) core, cyclic olefin copolymer (COC) working as waveguide cladding and insulating layer for the graphite–conductive polyethylene (gCPE) composite electrodes and finalized with polycarbonate outer cladding. The total diameter of the fiber is 200 μm. Bottom right: a head-mounted fixture for a fiber capable of simultaneous electrophysiology, drug delivery and optogenetics in tethered, behaving mice. **c**, Wireless, battery-free drug-delivery system combining four independently addressable drug reservoirs for programmed pharmacological neuromodulation in untethered, freely moving small animals such as mice. Inset; a mechanically compliant thin, flexible probe (500 μm wide, 50 μm thick) made of polydimethylsiloxane (PDMS) with a set of microfluidic channels (each with 10 × 10 μm^2 cross-section). This platform also includes μ-ILEDs (270 × 220 μm^2, 50 μm thick), collocated at the outlet of the microfluidic channels, for simultaneous optogenetic stimulation. Panels reproduced with permission from: **a**, ref. [89], The Royal Society of Chemistry; **b**, ref. [92], Springer Nature; **c**, ref. [94], PNAS.

excitatory pathways that are distinctive during motivated behavior, such as food consumption[103].

Additional possibilities in emerging approaches for electrochemical and optical sensing

The significance of the broad collection of neurotechnologies highlighted in previous sections increases further when considered in the context of emerging methodologies in neurobiology and synthetic biochemistry, specifically for neurochemical sensing. Discoveries in fluorescence[104,105], optogenetics[47,48] and electrochemical[106,107] sensing are of particular relevance. Conventional fluorescence approaches rely on genetically encoded FL probes that exploit fluorescent proteins (FPs), mainly GFP, as the fluorophore and either periplasmic-binding proteins or G-protein-coupled receptors as the target binding component[108] (Note: the term 'probe' here refers to the target binding entity, distinct from the use of this term in the context of technologies that appear in the other sections). Such probes traditionally rely on Förster resonance energy transfer (FRET) mechanisms where binding of a target changes the distance between a chromophore and a nearby quencher, thereby modulating the fluorescence efficiency. Most FPs include a rigid protein structure that protects the chromophore[109], with flexible regions for attaching target binding receptors, generally located far from the chromophore. These features restrict the movement of the quencher and chromophore upon target binding and result in probes with limited dynamic range and inability to detect analytes at low concentrations[110]. For example, Yellow Cameleon 6.1, a calcium probe, exhibits a dynamic range of ~200%, a dissociation constant (K_d) ~110 nM upon target binding, with typical response times (seconds) that are much slower than physiologically relevant calcium transients occurring on the scale of milliseconds[111].

Circularly permuted FPs (cpFPs) overcome these challenges. Here, the receptor exists within the primary structure of the FP, often in proximity to the chromophore without compromising the inherent fluorescence properties. Binding a target analyte to the cpFP thus results in large conformational changes and corresponding levels of modulation of the fluorescence, with speeds that can significantly exceed those achievable with FRET-based approaches (Fig. 8a)[112,113]. Comparisons of systems designed for the detection of calcium highlight advantages of cpFPs over FRET-based approaches. For example, calcium-selective GCAMP6f offers a dynamic range of >1,300%, K_d of ~375 nM and fast response time compared to FRET-based systems, approaching the timescales of naturally occurring transients[114].

Recent efforts expand the use of cpFPs to include detection of neurotransmitters. A family of dopamine-sensitive probes, dLight1, utilizes circularly permuted GFP incorporated in the third loop of human D1 receptor, to yield a positive feedback FL probe with a dynamic range of ~340% (Fig. 8b)[115]. In vivo studies in mice during dopamine transients induced by cue–reward learning tests illustrate the practical utility of these approaches as evaluated using conventional optical fibers (Fig. 8c). Similar strategies enable probes for GABA[116], dopamine[115], glutamate[117], acetylcholine[118], norepinephrine[119], ATP[120], glycine[121] and opioids[122].

Further prospects follow from FL probes that function at distinct wavelengths for wavelength-division multiplexed sensing and simultaneous optogenetics. Those that rely on near-infrared biliverdin-binding FL proteins represent interesting examples[123]. A calcium-sensitive near-infrared probe (NIR GECO1), as a negative-feedback FL probe, results from insertion of calmodulin (CaM)-RS20, a calcium-binding domain, into a biliverdin-binding monomeric infrared FL protein (mIFP; dynamic range ~90%; K_d ~215 nM). Here, binding changes the chromophore environment and decreases its fluorescence intensity (Fig. 8d–f)[124].

Recent developments in opsins for optogenetics create additional use cases. Of specific interest are step-function opsins with

ultra-high light sensitivity[125], due to their ability to function under low light intensity. From a technology standpoint, this result significantly reduces power requirements, with implications for device sizes, lifetimes and implantation strategies, and additional options in transcranial optical interfaces, as shown in mice and NHPs. Immediate opportunities are in systems that use collections of wireless, battery-free, implantable light sources and detectors, or multi-wavelength head-mounted microscopes, to track complex neurochemical processes and to optogenetically modulate neural activity in freely moving animals.

Important progress also extends to the development of electrochemical (EC) sensors. Standard approaches rely on tethered carbon microelectrodes and electroanalytical techniques for monitoring a relatively small collection of neurochemicals[126,127]. A recent paper describes a dual-functional wireless microneedle for simultaneous optogenetics and dopamine sensing[128]. The use of aptameric EC probes provides a route to expand the range of detectable species[129,130]. An aptamer for an EC sensor typically includes a redox moiety attached to the 3′-phosphate and a thiol linker at the 5′-phosphate group[130]. Binding of the target changes the distance between the redox moiety and the sensor electrode to create an electrical current with magnitude proportional to the concentration (Fig. 8g). A recent example involves aptamers functionalized with methylene blue as the redox moiety, bonded onto nanostructured Au microelectrodes (16 individual sites with diameters of 37 μm distributed along a silicon shank with 200 μm spacing) for monitoring cocaine in mice (K_d ~90 μM)[131] (Fig. 8h,i).

Advanced versions exploit aptamer-functionalized field-effect transistors, instead of passive electrodes[132]. Here the response follows from variations in the transconductance of the field effect transistors due to binding-induced electrostatic gating. This scheme eliminates the redox moiety and, more importantly, aligns the approach to silicon technologies similar to those in the active, high-density electronic platforms described in previous sections. Results that hint at future possibilities[132] use dopamine- (K_d ~150 nM) and serotonin- (K_d ~30 nM) selective aptamers functionalized onto silane-coated indium-oxide channel (thickness: 4 nm) formed over Au interdigitated electrodes (length: 1,500 μm; width: 80 μm) for selective detection of analytes in mouse brain tissue. Such schemes offer significant potential for neuroscience studies when combined with flexible electronic platforms and penetrating probes for large-area mapping of biochemically active species.

Conclusions

The neurotechnologies emphasized in this review (Box 1) are of interest because they facilitate important classes of neuroscience studies that lie outside of the scope of options supported by existing tools. The capabilities in neurological monitoring and

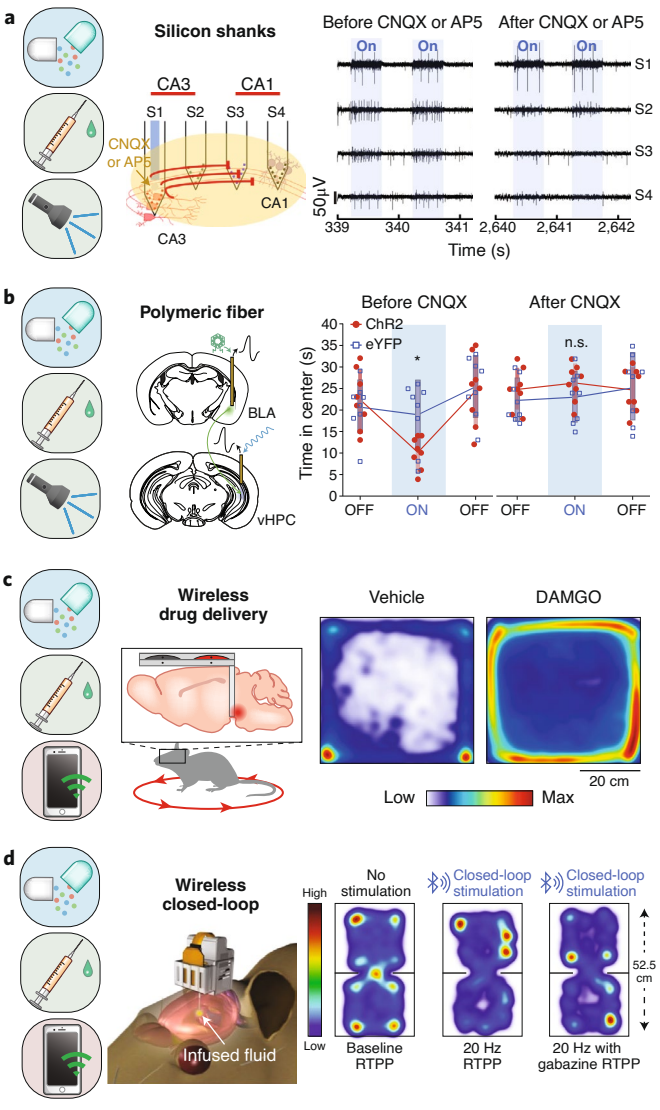

Fig. 7 | Uses of advanced platforms for programmed drug delivery in neuroscience research with animal models. a, Application of microfluidic drug delivery platforms on silicon shanks for the study of hippocampal CA1 and CA3 regions interactions in anaesthetized mice, to enhance understanding of processes of episodic and semantic memory consolidation, encoding and retrieval. Left: schematic illustration of the insertion of four shanks (S1, S2, S3 and S4) across CA1 and CA3 regions for electrophysiology recordings and one in CA3 for pharmacological delivery and optogenetic stimulation. Right: electrophysiology recordings from the four probes showing neuronal projections from CA3 to CA1 evoked by optogenetic stimulation, further inhibited by infusing the AMPA receptor antagonist CNQX and the NMDA receptor antagonist AP5 in CA3. **b**, Application of a multifunctional polymeric fiber for pharmacological and optogenetic modulation of anxiety behaviors in freely behaving mice. Left: schematic illustration of the strategy for anxiety modulation: ChR2 expressed in the BLA produces neuronal projections into the vHPC. Right: graph of data indicating that optogenetic stimulation of the BLA induces anxiety phenotypes in mice expressing ChR2, resulting in reductions in the time spent in the center of the open field test compared to the control group. Infusion of CNQX inhibits this neuronal projection pathway and thereby leads to a decrease in anxiety. **c**, Wireless, battery-free programmed pharmacological neuromodulation enables unique behavioral phenotype studies in untethered, freely moving small animal models. Left: unilateral pharmacological neuromodulation of the μ-opioid receptors with its agonist [D-Ala^2,*N*-Me-Phe^4,Gly^5-ol]-enkephalin (DAMGO) in the ventral tegmental area modulates contralateral rotation locomotion in mice. Right: heatmaps comparing the movement of a mouse when receiving a saline vehicle fluid (negative control; left) or DAMGO (positive control; right). **d**, Implementation of a wireless, closed-loop system for pharmacological and optogenetic stimulation using a battery-powered, low-energy Bluetooth device in an external, head-mounted configuration. Optogenetic stimulation of the LH in mice transfected with ChR2 induces real-time place-preference (RTPP) behavior, a phenotype that is suppressed by the pharmacological inhibition of GABA receptors. Left: schematic illustration of the device mounted on the head of a mouse. Right: heatmaps (from left to right) of the baseline for locomotion (without neuromodulation), during optogenetic stimulation before and after delivery of gabazine. Panels reproduced with permission from: **a**, ref. [91], Springer Nature; **b**, ref. [92], Springer Nature; **c**, ref. [94], PNAS. **d**, ref. [96], Springer Nature.

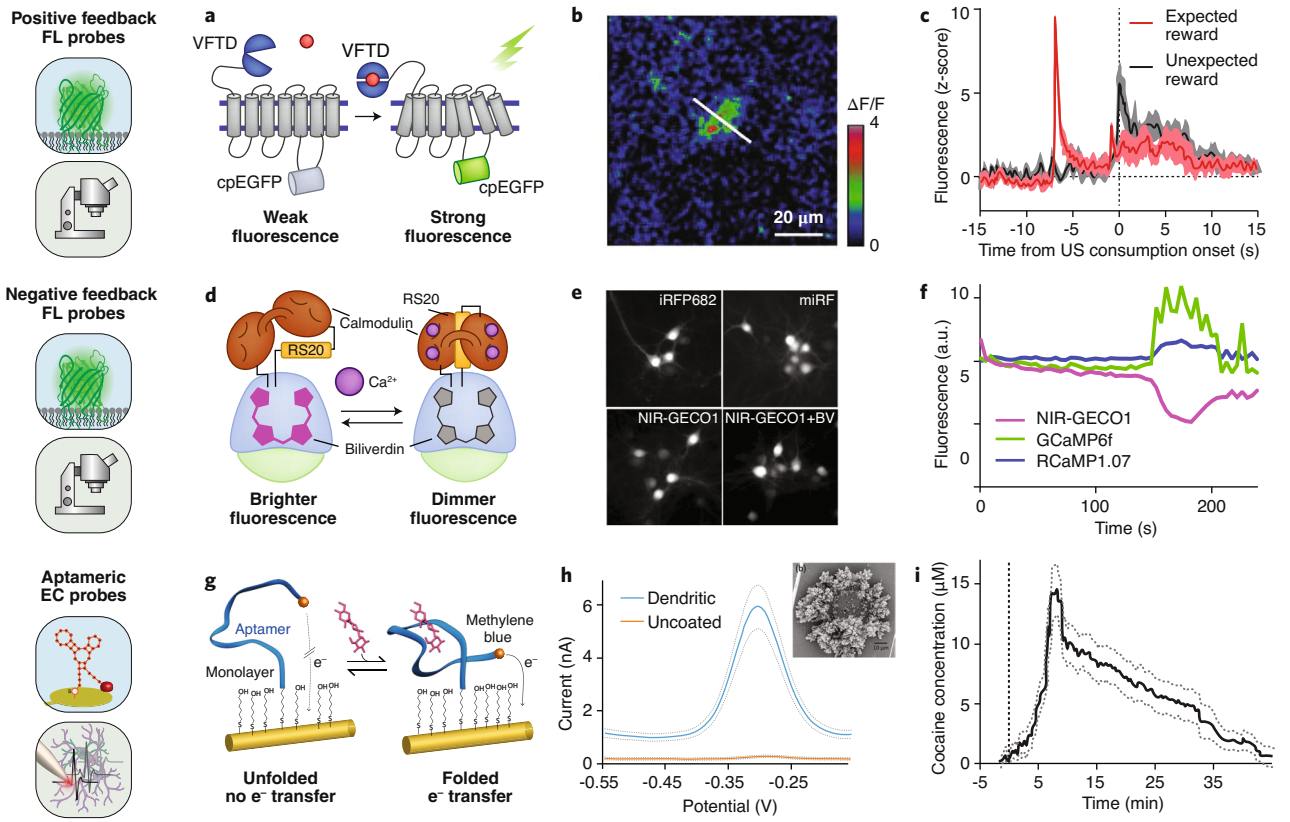

Fig. 8 | Emerging strategies for sensing of chemical biomarkers in vivo, and associated opportunities for advanced neurotechnology platforms. **a**, Schematic representation of a positive-feedback G-protein-coupled receptor-based FL sensor that exhibits an increase in fluorescence efficiency upon target binding. cpEGFP, circularly permuted enhanced GFP; VFTD, Venus flytrap domain. **b**, Two-photon microscope image of a representative fluorescence hotspot ($\Delta F/F$) associated with endogenous dopamine release in acute striatal slices evoked via electrical stimulus. **c**, Fluorescence response to unconditioned stimuli (US) during expected (red) versus unexpected (black) reward consumption ($n = 4$ mice) in a cue–reward extinction experiment. **d**, Working principle of a negative feedback near-infrared FL sensor for detecting Ca^{2+}, where the fluorescence efficiency decreases upon Ca^{2+} binding. RS20, synthetic calmodulin-binding peptide. **e**, Wide-field fluorescence images of mouse neurons expressing different versions of near-infrared-based fluorescence sensors (iRFP682, miRF, NIR-GECO1 and NIR-GECO1+BV) when exposed to 25 µM exogenous biliverdin. **f**, Simultaneous detection of spontaneous neuronal activity in a single cell co-expressing GCaMP6f, RCaMP1.07 and NIR-GECO1. **g**, A schematic illustration of the working principle of an aptamer-based electrochemical (EC) sensor in which analyte-binding induces a conformational change observed as an increase in electron (e^-) transfer to the electrode. **h**, Square wave voltammetry (SWV) response to methylene blue highlighting improved signal for an aptamer functionalized dendritic gold coated electrode (blue) compared to an analogous bare gold electrode (red). $n = 10$ individual electrodes for each average SWV response. Inset: SEM image of the dendritic gold-coated electrode. **i**, In vivo detection of the concentration of cocaine in the dorsal striatum of rats following systemic intravenous injection of cocaine (dose = 2 mg/kg, $n = 4$ electrodes from two independent rats). Panels reproduced with permission from: **a**, ref. [134], Frontiers Media SA; **b** and **c**, ref. [115], AAAS; **d**–**f**, ref. [124], Springer Nature; **g**, ref. [135], PNAS; **h** and **i**, ref. [131], The Royal Society of Chemistry.

neuromodulation may also eventually have relevance to human healthcare as advanced systems for addressing neurological disorders and various forms of organ dysfunction. Although these platforms offer many unique features for research purposes, overcoming certain remaining challenges may require further innovations. The foreign-body response is one of the main biological barriers for chronic implants. Mechanically compliant neurointerfaces and biocompatible materials are important, but the detailed and sometimes subtle characteristics of the biotic–abiotic interface can limit long-term stability. Miniaturization represents a general trend that will reduce these effects, but sometimes (e.g., electrical interfaces) at the expense of increased impedances and decreased signal quality. High-density data collection from miniaturized arrays also demands dedicated data acquisition systems that typically restrict applications to acute sessions with anaesthetized or restrained subjects. In addition, such electrical interfaces do not support cell-type-specific interrogation, as noted previously. Optogenetic interfaces do not have this limitation, but patterned, high-density illumination requires arrays of nano- or microscale light-emitting diodes or other advanced photonic schemes. Here, absorption and scattering properties of tissue must be considered as a fundamental limiting factor, likely constraining applications to shallow depths and short distances. Systems for microfluidic drug delivery are scalable to configurations at the micro- or nanoscale, but tissue scarring can lead to outlet clogging and potential tissue damage upon outlet bursting. Moreover, capabilities for multisite drug delivery at the single-neuron resolution will require additional concepts and development efforts.

Most of these neurotechnologies rely on wired connections for power delivery and data collection. Studies involving social behaviors among groups of animals using such systems are difficult or impossible to conduct, due either to adverse effects of the physical tethers or large headsets, both of which alter natural patterns of behavior and become targets of damage associated with activities (gnawing, scratching, etc.) of other animals. Wireless devices, especially those in fully implantable and battery-free designs, are thus

critically important. In fact, such systems now exist in deployable forms for optogenetics, photometry, oximetry, pharmacological delivery, temperature monitoring and even for measuring micro- and macrovascular blood flow. Related platforms for measuring heart rate, respiration rate, electrophysiological signals, concentrations of neurotransmitters and other parameters will emerge from ongoing development efforts in the near future, thereby dramatically expanding the range of possible neuroscience studies.

Additional opportunities for engineering research are in the context of biochemical sensing. In the case of optical sensors, cell internalization of cpFP and FRET-based FP probes during chronic studies is a major challenge that must be overcome. The low yields, high costs and time-consuming processes involved in developing such probes currently limit the pace of progress. Unique sets of additional difficulties exist for EC sensors. For example, routes for site-specific immobilization of different bioreceptors on high-density electrode arrays must be developed for multi-analyte, high resolution mapping. Moreover, deterioration of soft bioreceptors when interfaced with hard transducing sensor surfaces demands special attention. Challenges related to biofouling of sensor surfaces and resultant drifts in signal, degraded levels of reversibility and increased response times represent additional topics for continued work.

A goal for any such development effort is in technologies that can be translated to the research community and, in some cases, adapted for therapeutic use in humans. A number of government agencies, along with private equity firms and philanthropic organizations, support activities in these areas, with dedicated goals around revolutionizing our understanding of the human brain and/or creating associated commercial opportunities. An exciting recent example is the 3,072-channel neural interface formed with 192 filaments by the company Neuralink[133] as a potential computer interface and clinical therapy tool for neurological diseases. A convergence of efforts, fostered by academy-industry consortia, will help to promote the development and dissemination of these and other types of technologies as widely accessible tools for the neuroscience community, with profound implications for the field of brain science.

Received: 26 June 2020; Accepted: 9 October 2020;
Published online: 16 November 2020

References

1. Brenner, S. & Sejnowski, T. J. Understanding the human brain. *Science* **334**, 567 (2011).
2. Bouthour, W. et al. Biomarkers for closed-loop deep brain stimulation in Parkinson disease and beyond. *Nat. Rev. Neurol.* **15**, 343–352 (2019).
3. Yang, X. et al. Bioinspired neuron-like electronics. *Nat. Mater.* **18**, 510–517 (2019).
4. Hong, G. et al. A method for single-neuron chronic recording from the retina in awake mice. *Science* **360**, 1447–1451 (2018).
5. Muskovich, M. & Bettinger, C. J. Biomaterials-based electronics: polymers and interfaces for biology and medicine. *Adv. Healthc. Mater.* **1**, 248–266 (2012).
6. Rochford, A. E., Carnicer-Lombarte, A., Curto, V. F., Malliaras, G. G. & Barone, D. G. When bio meets technology: biohybrid neural interfaces. *Adv. Mater.* **32**, e1903182 (2020).
7. Tsai, D., Sawyer, D., Bradd, A., Yuste, R. & Shepard, K. L. A very large-scale microelectrode array for cellular-resolution electrophysiology. *Nat. Commun.* **8**, 1802 (2017).
8. Wu, X. et al. Sono-optogenetics facilitated by a circulationdelivered rechargeable light source for minimally invasive optogenetics. *Proc. Natl. Acad. Sci. USA* **116**, 26332–26342 (2019).
9. Chen, R., Romero, G., Christiansen, M. G., Mohr, A. & Anikeeva, P. Wireless magnetothermal deep brain stimulation. *Science* **347**, 1477–1480 (2015).
10. Zhang, M. et al. Bright quantum dots emitting at ~1,600 nm in the NIR-IIb window for deep tissue fluorescence imaging. *Proc. Natl. Acad. Sci. USA* **115**, 6590–6595 (2018).
11. Liu, J. et al. A sensitive and specific nanosensor for monitoring extracellular potassium levels in the brain. *Nat. Nanotechnol.* **15**, 321–330 (2020).
12. Mohanty, A. et al. Reconfigurable nanophotonic silicon probes for sub-millisecond deep-brain optical stimulation. *Nat. Biomed. Eng.* **4**, 223–231 (2020).
13. Seo, D. et al. Wireless recording in the peripheral nervous system with ultrasonic neural dust. *Neuron* **91**, 529–539 (2016).
14. Hong, G. & Lieber, C. M. Novel electrode technologies for neural recordings. *Nat. Rev. Neurosci.* **20**, 330–345 (2019).
15. Lacour, S. P., Courtine, G. & Guck, J. Materials and technologies for soft implantable neuroprostheses. *Nat. Rev. Mater.* **1**, 16063 (2016).
16. Jastrzebska-Perfect, P. et al. Translational neuroelectronics. *Adv. Funct. Mater.* **30**, 1909165 (2020).
17. Salatino, J. W., Ludwig, K. A., Kozai, T. D. Y. & Purcell, E. K. Glial responses to implanted electrodes in the brain. *Nat. Biomed. Eng.* **1**, 862–877 (2017).
18. Viswam, V., Obien, M. E. J., Franke, F., Frey, U. & Hierlemann, A. Optimal electrode size for multi-scale extracellular-potential recording from neuronal assemblies. *Front. Neurosci.* **13**, 385 (2019).
19. Cogan, S. F. Neural stimulation and recording electrodes. *Annu. Rev. Biomed. Eng.* **10**, 275–309 (2008).
20. Tybrandt, K. et al. High-density stretchable electrode grids for chronic neural recording. *Adv. Mater.* **30**, e1706520 (2018).
21. Minev, I. R. et al. Biomaterials. Electronic dura mater for long-term multimodal neural interfaces. *Science* **347**, 159–163 (2015).
22. Liu, Y. et al. Soft and elastic hydrogel-based microelectronics for localized low-voltage neuromodulation. *Nat. Biomed. Eng.* **3**, 58–68 (2019).
23. Qi, D. et al. Highly stretchable, compliant, polymeric microelectrode arrays for in vivo electrophysiological interfacing. *Adv. Mater.* **29**, 1–10 (2017).
24. Guo, L., Ma, M., Zhang, N., Langer, R. & Anderson, D. G. Stretchable polymeric multielectrode array for conformal neural interfacing. *Adv. Mater.* **26**, 1427–1433 (2014).
25. Aqrawe, Z., Montgomery, J., Travas-Sejdic, J. & Svirskis, D. Conducting polymers for neuronal microelectrode array recording and stimulation. *Sens. Actuators B Chem.* **257**, 753–765 (2018).
26. Rogers, J. A., Someya, T. & Huang, Y. Materials and mechanics for stretchable electronics. *Science* **327**, 1603–1607 (2010).
27. Khodagholy, D. et al. NeuroGrid: recording action potentials from the surface of the brain. *Nat. Neurosci.* **18**, 310–315 (2015).
28. Escabí, M. A. et al. A high-density, high-channel count, multiplexed μECoG array for auditory-cortex recordings. *J. Neurophysiol.* **112**, 1566–1583 (2014).
29. Chiang, C.-H. et al. Development of a neural interface for high-definition, long-term recording in rodents and nonhuman primates. *Sci. Transl. Med.* **12**, eaay4682 (2020).
30. Viventi, J. et al. Flexible, foldable, actively multiplexed, high-density electrode array for mapping brain activity in vivo. *Nat. Neurosci.* **14**, 1599–1605 (2011).
31. Campbell, P. K., Jones, K. E., Huber, R. J., Horch, K. W. & Normann, R. A. A silicon-based, three-dimensional neural interface: manufacturing processes for an intracortical electrode array. *IEEE Trans. Biomed. Eng.* **38**, 758–768 (1991).
32. Drake, K. L., Wise, K. D., Farraye, J., Anderson, D. J. & BeMent, S. L. Performance of planar multisite microprobes in recording extracellular single-unit intracortical activity. *IEEE Trans. Biomed. Eng.* **35**, 719–732 (1988).
33. Mora Lopez, C. et al. A neural probe with up to 966 electrodes and up to 384 configurable channels in 0.13 μm SOI CMOS. *IEEE Trans. Biomed. Circuits Syst.* **11**, 510–522 (2017).
34. Jun, J. J. et al. Fully integrated silicon probes for high-density recording of neural activity. *Nature* **551**, 232–236 (2017).
35. Scholvin, J. et al. Close-packed silicon microelectrodes for scalable spatially oversampled neural recording. *IEEE Trans. Biomed. Eng.* **63**, 120–130 (2016).
36. Kwon, K. Y., Sirowatka, B., Weber, A. & Li, W. Opto- μECoG array: a hybrid neural interface with transparent μECoG electrode array and integrated LEDs for optogenetics. *IEEE Trans. Biomed. Circuits Syst.* **7**, 593–600 (2013).
37. Park, D. W. et al. Graphene-based carbon-layered electrode array technology for neural imaging and optogenetic applications. *Nat. Commun.* **5**, 5258 (2014).
38. Lee, J., Ozden, I., Song, Y. K. & Nurmikko, A. V. Transparent intracortical microprobe array for simultaneous spatiotemporal optical stimulation and multichannel electrical recording. *Nat. Methods* **12**, 1157–1162 (2015).
39. Qiang, Y. et al. Transparent arrays of bilayer-nanomesh microelectrodes for simultaneous electrophysiology and two-photon imaging in the brain. *Sci. Adv.* **4**, t0626 (2018).
40. Lee, W. et al. Transparent, conformable, active multielectrode array using organic electrochemical transistors. *Proc. Natl. Acad. Sci. USA* **114**, 10554–10559 (2017).
41. Nir, Y. et al. Regional slow waves and spindles in human sleep. *Neuron* **70**, 153–169 (2011).
42. Buzsáki, G. & Draguhn, A. Neuronal oscillations in cortical networks. *Science* **304**, 1926–1929 (2004).
43. Lewis, C. M., Bosman, C. A. & Fries, P. Recording of brain activity across spatial scales. *Curr. Opin. Neurobiol.* **32**, 68–77 (2015).

44. Steinmetz, N. A., Zatka-Haas, P., Carandini, M. & Harris, K. D. Distributed coding of choice, action and engagement across the mouse brain. *Nature* **576**, 266–273 (2019).
45. Vinck, M., Batista-Brito, R., Knoblich, U. & Cardin, J. A. Arousal and locomotion make distinct contributions to cortical activity patterns and visual encoding. *Neuron* **86**, 740–754 (2015).
46. Boyden, E. S., Zhang, F., Bamberg, E., Nagel, G. & Deisseroth, K. Millisecond-timescale, genetically targeted optical control of neural activity. *Nat. Neurosci.* **8**, 1263–1268 (2005).
47. Fenno, L., Yizhar, O. & Deisseroth, K. The development and application of optogenetics. *Annu. Rev. Neurosci.* **34**, 389–412 (2011).
48. Yizhar, O., Fenno, L. E., Davidson, T. J., Mogri, M. & Deisseroth, K. Optogenetics in neural systems. *Neuron* **71**, 9–34 (2011).
49. Miyamoto, D. & Murayama, M. The fiber-optic imaging and manipulation of neural activity during animal behavior. *Neurosci. Res.* **103**, 1–9 (2016).
50. Pisano, F. et al. Depth-resolved fiber photometry with a single tapered optical fiber implant. *Nat. Methods* **16**, 1185–1192 (2019).
51. Pisanello, F. et al. Dynamic illumination of spatially restricted or large brain volumes via a single tapered optical fiber. *Nat. Neurosci.* **20**, 1180–1188 (2017).
52. Pisanello, F. et al. Multipoint-emitting optical fibers for spatially addressable in vivo optogenetics. *Neuron* **82**, 1245–1254 (2014).
53. Segev, E. et al. Patterned photostimulation via visible-wavelength photonic probes for deep brain optogenetics. *Neurophotonics* **4**, 011002 (2017).
54. Zorzos, A. N., Boyden, E. S. & Fonstad, C. G. Multiwaveguide implantable probe for light delivery to sets of distributed brain targets. *Opt. Lett.* **35**, 4133–4135 (2010).
55. Buzsáki, G. et al. Tools for probing local circuits: high-density silicon probes combined with optogenetics. *Neuron* **86**, 92–105 (2015).
56. Seymour, J. P., Wu, F., Wise, K. D. & Yoon, E. State-of-the-art MEMS and microsystem tools for brain research. *Microsyst. Nanoeng.* **3**, 16066 (2017).
57. Wu, F. et al. Monolithically integrated μLEDs on silicon neural probes for high-resolution optogenetic studies in behaving animals. *Neuron* **88**, 1136–1148 (2015).
58. Won, S. M. et al. Recent advances in materials, devices, and systems for neural interfaces. *Adv. Mater.* **30**, e1800534 (2018).
59. Qazi, R., Kim, C. Y., Byun, S. H. & Jeong, J. W. Microscale inorganic LED based wireless neural systems for chronic in vivo optogenetics. *Front. Neurosci.* **12**, 764 (2018).
60. Kim, T. I. et al. Injectable, cellular-scale optoelectronics with applications for wireless optogenetics. *Science* **340**, 211–216 (2013).
61. Shin, G. et al. Flexible near-field wireless optoelectronics as subdermal implants for broad applications in optogenetics. *Neuron* **93**, 509–521.e3 (2017).
62. Montgomery, K. L. et al. Wirelessly powered, fully internal optogenetics for brain, spinal and peripheral circuits in mice. *Nat. Methods* **12**, 969–974 (2015).
63. Samineni, V. K. et al. Optogenetic silencing of nociceptive primary afferents reduces evoked and ongoing bladder pain. *Sci. Rep.* **7**, 15865 (2017).
64. Mickle, A. D. et al. A wireless closed-loop system for optogenetic peripheral neuromodulation. *Nature* **565**, 361–365 (2019).
65. Gutruf, P. et al. Wireless, battery-free, fully implantable multimodal and multisite pacemakers for applications in small animal models. *Nat. Commun.* **10**, 5742 (2019).
66. Samineni, V. K. et al. Fully implantable, battery-free wireless optoelectronic devices for spinal optogenetics. *Pain* **158**, 2108–2116 (2017).
67. Lu, L. et al. Wireless optoelectronic photometers for monitoring neuronal dynamics in the deep brain. *Proc. Natl. Acad. Sci. USA* **115**, E1374–E1383 (2018).
68. Hibberd, T. J. et al. Optogenetic Induction of Colonic Motility in Mice. *Gastroenterology* **155**, 514–528.e6 (2018).
69. Park, S. I. et al. Soft, stretchable, fully implantable miniaturized optoelectronic systems for wireless optogenetics. *Nat. Biotechnol.* **33**, 1280–1286 (2015).
70. Gutruf, P. et al. Fully implantable optoelectronic systems for battery-free, multimodal operation in neuroscience research. *Nat. Electron.* **1**, 652–660 (2018).
71. Burton, A. et al. Wireless, battery-free subdermally implantable photometry systems for chronic recording of neural dynamics. *Proc. Natl. Acad. Sci. USA* **117**, 2835–2845 (2020).
72. Zhang, H. et al. Wireless, battery-free optoelectronic systems as subdermal implants for local tissue oximetry. *Sci. Adv.* **5**, w0873 (2019).
73. Grienberger, C. & Konnerth, A. Imaging calcium in neurons. *Neuron* **73**, 862–885 (2012).
74. Skocek, O. et al. High-speed volumetric imaging of neuronal activity in freely moving rodents. *Nat. Methods* **15**, 429–432 (2018).
75. Ghosh, K. K. et al. Miniaturized integration of a fluorescence microscope. *Nat. Methods* **8**, 871–878 (2011).
76. Zong, W. et al. Fast high-resolution miniature two-photon microscopy for brain imaging in freely behaving mice. *Nat. Methods* **14**, 713–719 (2017).
77. Benninger, R. K. P. & Piston, D. W. Two-photon excitation microscopy for the study of living cells and tissues. *Curr. Protoc. Cell Biol.* **Chapter 4**, 1–24 (2013).
78. Wang, T. et al. Three-photon imaging of mouse brain structure and function through the intact skull. *Nat. Methods* **15**, 789–792 (2018).
79. Villette, V. et al. Ultrafast two-photon imaging of a high-gain voltage indicator in awake behaving mice. *Cell* **179**, 1590–1608.e23 (2019).
80. Yang, W., Carrillo-Reid, L., Bando, Y., Peterka, D. S. & Yuste, R. Simultaneous two-photon imaging and two-photon optogenetics of cortical circuits in three dimensions. *eLife* **7**, 1–21 (2018).
81. Packer, A. M., Russell, L. E., Dalgleish, H. W. P. & Häusser, M. Simultaneous all-optical manipulation and recording of neural circuit activity with cellular resolution in vivo. *Nat. Methods* **12**, 140–146 (2015).
82. Acker, L. C., Pino, E. N., Boyden, E. S. & Desimone, R. Large volume, behaviorally-relevant illumination for optogenetics in nonhuman primates. *J. Vis. Exp.* **2017**, 56330 (2017).
83. Acker, L., Pino, E. N., Boyden, E. S. & Desimone, R. FEF inactivation with improved optogenetic methods. *Proc. Natl. Acad. Sci. USA* **113**, E7297–E7306 (2016).
84. English, D. F. et al. Pyramidal cell-interneuron circuit architecture and dynamics in hippocampal networks. *Neuron* **96**, 505–520.e7 (2017).
85. Scott, B. B. et al. Imaging cortical dynamics in GCaMP transgenic rats with a head-mounted widefield macroscope. *Neuron* **100**, 1045–1058.e5 (2018).
86. Kondo, T. et al. Calcium transient dynamics of neural ensembles in the primary motor cortex of naturally behaving monkeys. *Cell Rep.* **24**, 2191–2195.e4 (2018).
87. Kim, D. H. et al. Pan-neuronal calcium imaging with cellular resolution in freely swimming zebrafish. *Nat. Methods* **14**, 1107–1114 (2017).
88. Lee, H. J. et al. A multichannel neural probe with embedded microfluidic channels for simultaneous in vivo neural recording and drug delivery. *Lab Chip* **15**, 1590–1597 (2015).
89. Shin, H. et al. Neural probes with multi-drug delivery capability. *Lab Chip* **15**, 3730–3737 (2015).
90. Lee, W. H., Slaney, T. R., Hower, R. W. & Kennedy, R. T. Microfabricated sampling probes for in vivo monitoring of neurotransmitters. *Anal. Chem.* **85**, 3828–3831 (2013).
91. Shin, H. et al. Multifunctional multi-shank neural probe for investigating and modulating long-range neural circuits in vivo. *Nat. Commun.* **10**, 3777 (2019).
92. Park, S. et al. One-step optogenetics with multifunctional flexible polymer fibers. *Nat. Neurosci.* **20**, 612–619 (2017).
93. Jeong, J. W. et al. Wireless optofluidic systems for programmable in vivo pharmacology and optogenetics. *Cell* **162**, 662–674 (2015).
94. Zhang, Y. et al. Battery-free, lightweight, injectable microsystem for in vivo wireless pharmacology and optogenetics. *Proc. Natl. Acad. Sci. USA* **116**, 21427–21437 (2019).
95. Noh, K. N. et al. Miniaturized, battery-free optofluidic systems with potential for wireless pharmacology and optogenetics. *Small* **14**, 1–8 (2018).
96. Qazi, R. et al. Wireless optofluidic brain probes for chronic neuropharmacology and photostimulation. *Nat. Biomed. Eng.* **3**, 655–669 (2019).
97. Zhang, Y. et al. Battery-free, fully implantable optofluidic cuff system for wireless optogenetic and pharmacological neuromodulation of peripheral nerves. *Sci. Adv.* **5**, w5296 (2019).
98. McCall, J. G. et al. Preparation and implementation of optofluidic neural probes for in vivo wireless pharmacology and optogenetics. *Nat. Protoc.* **12**, 219–237 (2017).
99. Leutgeb, S., Leutgeb, J. K., Treves, A., Moser, M. B. & Moser, E. I. Distinct ensemble codes in hippocampal areas CA3 and CA1. *Science* **305**, 1295–1298 (2004).
100. Pereira, A. et al. Processing of tactile information by the hippocampus. *Proc. Natl. Acad. Sci. USA* **104**, 18286–18291 (2007).
101. Felix-Ortiz, A. C. et al. BLA to vHPC inputs modulate anxiety-related behaviors. *Neuron* **79**, 658–664 (2013).
102. Devine, D. P. & Wise, R. A. Self-administration of morphine, DAMGO, and DPDPE into the ventral tegmental area of rats. *J. Neurosci.* **14**, 1978–1984 (1994).
103. Jennings, J. H., Rizzi, G., Stamatakis, A. M., Ung, R. L. & Stuber, G. D. The inhibitory circuit architecture of the lateral hypothalamus orchestrates feeding. *Science* **341**, 1517–1521 (2013).
104. O'Banion, C. P. & Yasuda, R. Fluorescent sensors for neuronal signaling. *Curr. Opin. Neurobiol.* **63**, 31–41 (2020).
105. Shen, Y., Nasu, Y., Shkolnikov, I., Kim, A. & Campbell, R. E. Engineering genetically encoded fluorescent indicators for imaging of neuronal activity: progress and prospects. *Neurosci. Res.* **152**, 3–14 (2020).
106. Ganesana, M., Lee, S. T., Wang, Y. & Venton, B. J. Analytical techniques in neuroscience: recent advances in imaging, separation, and electrochemical methods. *Anal. Chem.* **89**, 314–341 (2017).

107. Tavakolian-Ardakani, Z., Hosu, O., Cristea, C., Mazloum-Ardakani, M. & Marrazza, G. Latest trends in electrochemical sensors for neurotransmitters: a review. *Sensors (Basel)* **19**, 2037 (2019).
108. Lin, M. Z. & Schnitzer, M. J. Genetically encoded indicators of neuronal activity. *Nat. Neurosci.* **19**, 1142–1153 (2016).
109. Ward, W. W. & Bokman, S. H. Reversible denaturation of *Aequorea* green-fluorescent protein: physical separation and characterization of the renatured protein. *Biochemistry* **21**, 4535–4540 (1982).
110. Kostyuk, A. I., Demidovich, A. D., Kotova, D. A., Belousov, V. V. & Bilan, D. S. Circularly permuted fluorescent protein-based indicators: history, principles, and classification. *Int. J. Mol. Sci.* **20**, 4200 (2019).
111. Truong, K. et al. FRET-based in vivo Ca^{2+} imaging by a new calmodulin-GFP fusion molecule. *Nat. Struct. Biol.* **8**, 1069–1073 (2001).
112. Lee, Y.-T., He, L. & Zhou, Y. Expanding the chemogenetic toolbox by circular permutation. *J. Mol. Biol.* **432**, 3127–3136 (2020).
113. Bajar, B. T., Wang, E. S., Zhang, S., Lin, M. Z. & Chu, J. A guide to fluorescent protein FRET pairs. *Sensors (Basel)* **16**, 1488 (2016).
114. Chen, T.-W. et al. Ultrasensitive fluorescent proteins for imaging neuronal activity. *Nature* **499**, 295–300 (2013).
115. Patriarchi, T. et al. Ultrafast neuronal imaging of dopamine dynamics with designed genetically encoded sensors. *Science* **360**, eaat4422 (2018).
116. Marvin, J. S. et al. A genetically encoded fluorescent sensor for in vivo imaging of GABA. *Nat. Methods* **16**, 763–770 (2019).
117. Helassa, N. et al. Ultrafast glutamate sensors resolve high-frequency release at Schaffer collateral synapses. *Proc. Natl. Acad. Sci. USA* **115**, 5594–5599 (2018).
118. Jing, M. et al. A genetically encoded fluorescent acetylcholine indicator for in vitro and in vivo studies. *Nat. Biotechnol.* **36**, 726–737 (2018).
119. Feng, J. et al. A genetically encoded fluorescent sensor for rapid and specific in vivo detection of norepinephrine. *Neuron* **102**, 745–761.e8 (2019).
120. Lobas, M. A. et al. A genetically encoded single-wavelength sensor for imaging cytosolic and cell surface ATP. *Nat. Commun.* **10**, 711 (2019).
121. Zhang, W. H. et al. Monitoring hippocampal glycine with the computationally designed optical sensor GlyFS. *Nat. Chem. Biol.* **14**, 861–869 (2018).
122. Stoeber, M. et al. A genetically encoded biosensor reveals location bias of opioid drug action. *Neuron* **98**, 963–976.e5 (2018).
123. Chernov, K. G., Redchuk, T. A., Omelina, E. S. & Verkhusha, V. V. Near-infrared fluorescent proteins, biosensors, and optogenetic tools engineered from phytochromes. *Chem. Rev.* **117**, 6423–6446 (2017).
124. Qian, Y. et al. A genetically encoded near-infrared fluorescent calcium ion indicator. *Nat. Methods* **16**, 171–174 (2019).
125. Gong, X. et al. An ultra-sensitive step-function opsin for minimally invasive optogenetic stimulation in mice and macaques. *Neuron* **107**, 38–51.e8 (2020).
126. Ribeiro, J. A., Fernandes, P. M. V., Pereira, C. M. & Silva, F. Electrochemical sensors and biosensors for determination of catecholamine neurotransmitters: A review. *Talanta* **160**, 653–679 (2016).
127. Bucher, E. S. & Wightman, R. M. Electrochemical analysis of neurotransmitters. *Annu. Rev. Anal. Chem. (Palo Alto Calif.)* **8**, 239–261 (2015).
128. Liu, C. et al. A wireless, implantable optoelectrochemical probe for optogenetic stimulation and dopamine detection. *Microsyst. Nanoeng.* **6**, 64 (2020).
129. Xiao, Y., Piorek, B. D., Plaxco, K. W. & Heeger, A. J. A reagentless signal-on architecture for electronic, aptamer-based sensors via target-induced strand displacement. *J. Am. Chem. Soc.* **127**, 17990–17991 (2005).
130. Schoukroun-Barnes, L. R. et al. Reagentless, structure-switching, electrochemical aptamer-based sensors. *Annu. Rev. Anal. Chem. (Palo Alto Calif.)* **9**, 163–181 (2016).
131. Taylor, I. M. et al. Aptamer-functionalized neural recording electrodes for the direct measurement of cocaine in vivo. *J. Mater. Chem. B Mater. Biol. Med.* **5**, 2445–2458 (2017).
132. Nakatsuka, N. et al. Aptamer-field-effect transistors overcome Debye length limitations for small-molecule sensing. *Science* **362**, 319–324 (2018).
133. Musk, E. An integrated brain-machine interface platform with thousands of channels. *J. Med. Internet Res.* **21**, e16194 (2019).
134. Leopold, A. V., Shcherbakova, D. M. & Verkhusha, V. V. Fluorescent biosensors for neurotransmission and neuromodulation: engineering and applications. *Front. Cell. Neurosci.* **13**, 474 (2019).
135. Arroyo-Currás, N. et al. Real-time measurement of small molecules directly in awake, ambulatory animals. *Proc. Natl. Acad. Sci. USA* **114**, 645–650 (2017).
136. Strumwasser, F. Long-term recording' from single neurons in brain of unrestrained mammals. *Science* **127**, 469–470 (1958).
137. McNaughton, B. L., O'Keefe, J. & Barnes, C. A. The stereotrode: a new technique for simultaneous isolation of several single units in the central nervous system from multiple unit records. *J. Neurosci. Methods* **8**, 391–397 (1983).
138. Hodgkin, A. L. & Huxley, A. F. Action potentials recorded from inside a nerve fibre. *Nature* **144**, 710–711 (1939).
139. Buzsáki, G., Anastassiou, C. A. & Koch, C. The origin of extracellular fields and currents—EEG, ECoG, LFP and spikes. *Nat. Rev. Neurosci.* **13**, 407–420 (2012).
140. Song, E., Li, J., Won, S. M., Bai, W. & Rogers, J. A. Materials for flexible bioelectronic systems as chronic neural interfaces. *Nat. Mater.* **19**, 590–603 (2020).
141. Armbruster, B. N., Li, X., Pausch, M. H., Herlitze, S. & Roth, B. L. Evolving the lock to fit the key to create a family of G protein-coupled receptors potently activated by an inert ligand. *Proc. Natl. Acad. Sci. USA* **104**, 5163–5168 (2007).
142. Alexander, G. M. et al. Remote control of neuronal activity in transgenic mice expressing evolved G protein-coupled receptors. *Neuron* **63**, 27–39 (2009).
143. Banghart, M. R. & Sabatini, B. L. Photoactivatable neuropeptides for spatiotemporally precise delivery of opioids in neural tissue. *Neuron* **73**, 249–259 (2012).
144. Hüll, K., Morstein, J. & Trauner, D. In vivo photopharmacology. *Chem. Rev.* **118**, 10710–10747 (2018).
145. Luo, L., Callaway, E. M. & Svoboda, K. Genetic dissection of neural circuits. *Neuron* **57**, 634–660 (2008).
146. Magnus, C. J. et al. Chemical and genetic engineering of selective ion channel-ligand interactions. *Science* **333**, 1292–1296 (2011).
147. Roth, B. L. DREADDs for neuroscientists. *Neuron* **89**, 683–694 (2016).
148. Dana, H. et al. Sensitive red protein calcium indicators for imaging neural activity. *eLife* **5**, 1–24 (2016).
149. Piatkevich, K. D. et al. A robotic multidimensional directed evolution approach applied to fluorescent voltage reporters. *Nat. Chem. Biol.* **14**, 352–360 (2018).
150. Zou, P. et al. Bright and fast multicoloured voltage reporters via electrochromic FRET. *Nat. Commun.* **5**, 4625 (2014).

Acknowledgements

This research was supported by the Querrey Simpson Institute for Bioelectronics at Northwestern University.

Author contributions

A.V.-G., Y.Y., A.J.B., and J.A.R. cowrote and co-edited the manuscript.

Competing interests

J.A.R. is cofounder in a company, Neurolux Inc., that offers related technology products to the neuroscience community.

Additional information

Correspondence should be addressed to J.A.R.

Peer review information Nature Neuroscience thanks Sebastian Haesler and the other, anonymous, reviewer(s) for their contribution to the peer review of this work.